


RESEARCH

Open Access



# Identification of RNA reads encoding different channels in isolated rat ventricular myocytes and the effect of cell stretching on *L-type* $Ca^{2+}$ current

Andre G. Kamkin<sup>1</sup>, Olga V. Kamkina<sup>1</sup>, Viktor E. Kazansky<sup>1</sup>, Vadim M. Mitrokhin<sup>1</sup>, Andrey Bilichenko<sup>1</sup>, Elizaveta A. Nasedkina<sup>1</sup>, Stanislav A. Shileiko<sup>1</sup>, Anastasia S. Rodina<sup>1</sup>, Alexandra D. Zolotareva<sup>1</sup>, Valentin I. Zolotarev<sup>1</sup>, Pavel V. Sutyagin<sup>1</sup> and Mitko I. Mladenov<sup>1,2\*</sup> 

## Abstract

**Background** The study aimed to identify transcripts of specific ion channels in rat ventricular cardiomyocytes and determine their potential role in the regulation of ionic currents in response to mechanical stimulation. The gene expression levels of various ion channels in freshly isolated rat ventricular cardiomyocytes were investigated using the RNA-seq technique. We also measured changes in current through  $Ca_v1.2$  channels under cell stretching using the whole-cell patch-clamp method.

**Results** Among channels that showed mechanosensitivity, significant amounts of TRPM7, TRPC1, and TRPM4 transcripts were found. We suppose that the recorded *L-type*  $Ca^{2+}$  current is probably expressed through  $Ca_v1.2$ . Furthermore, stretching cells by 6, 8, and 10  $\mu\text{m}$ , which increases  $I_{SAC}$  through the TRPM7, TRPC1, and TRPM4 channels, also decreased  $I_{Ca,L}$  through the  $Ca_v1.2$  channels in  $K^+_{in}/K^+_{out}$ ,  $Cs^+_{in}/K^+_{out}$ ,  $K^+_{in}/Cs^+_{out}$ , and  $Cs^+_{in}/Cs^+_{out}$  solutions. The application of a nonspecific  $I_{SAC}$  blocker,  $Gd^{3+}$ , during cell stretching eliminated  $I_{SAC}$  through nonselective cation channels and  $I_{Ca,L}$  through  $Ca_v1.2$  channels. Since the response to  $Gd^{3+}$  was maintained in  $Cs^+_{in}/Cs^+_{out}$  solutions, we suggest that voltage-gated  $Ca_v1.2$  channels in the ventricular myocytes of adult rats also exhibit mechanosensitive properties.

**Conclusions** Our findings suggest that TRPM7, TRPC1, and TRPM4 channels represent stretch-activated nonselective cation channels in rat ventricular myocytes. Probably the  $Ca_v1.2$  channels in these cells exhibit mechanosensitive properties. Our results provide insight into the molecular mechanisms underlying stretch-induced responses in rat ventricular myocytes, which may have implications for understanding cardiac physiology and pathophysiology.

**Keywords** Rat ventricular myocytes, Mechanosensitive cation channels, Stretch-activated channels, mRNA, Transcriptomic profile,  $Ca_v1.2$  channels

\*Correspondence:  
Mitko I. Mladenov  
mitkom@pmf.ukim.mk

<sup>1</sup>Department of Physiology, Pirogov Russian National Research Medical University, Moscow, Russian Federation

<sup>2</sup>Faculty of Natural Sciences and Mathematics, Institute of Biology, "Ss. Cyril and Methodius" University, Skopje, North, Macedonia



© The Author(s) 2023. **Open Access** This article is licensed under a Creative Commons Attribution 4.0 International License, which permits use, sharing, adaptation, distribution and reproduction in any medium or format, as long as you give appropriate credit to the original author(s) and the source, provide a link to the Creative Commons licence, and indicate if changes were made. The images or other third party material in this article are included in the article's Creative Commons licence, unless indicated otherwise in a credit line to the material. If material is not included in the article's Creative Commons licence and your intended use is not permitted by statutory regulation or exceeds the permitted use, you will need to obtain permission directly from the copyright holder. To view a copy of this licence, visit <http://creativecommons.org/licenses/by/4.0/>. The Creative Commons Public Domain Dedication waiver (<http://creativecommons.org/publicdomain/zero/1.0/>) applies to the data made available in this article, unless otherwise stated in a credit line to the data.

## Background

During the last five decades, scientists have collected a lot of evidence that mechanical stress has a significant impact on the electrophysiological properties of cardiomyocytes. This phenomenon, commonly referred to as mechanoelectric feedback, has been extensively studied [1] and is believed to play a crucial role in the pathophysiology of cardiac arrhythmias [2, 3]. In healthy hearts, this feedback mechanism can involve transmembrane cation fluxes through stretch-activated channels (SACs) [4], which can modulate the membrane potential of cardiac myocytes [5–7]. Scientific data have shown that localized stretching of single ventricular or atrial myocytes involves cation flux through cation-nonselective SACs [5], which in turn can affect the membrane potential of these cells. Stretch sensitivity is particularly high in hypertrophied ventricular cardiomyocytes from spontaneously hypertensive rats and in atrial and ventricular cardiomyocytes from patients with end-stage heart failure [8]. In general, the role of cardiomyocyte SACs is not limited to normal heart function but also plays a crucial role in various pathological conditions.

Several studies reported  $\text{Ca}^{2+}$  as well as  $\text{Na}^+$  and  $\text{K}^+$  permeability in SACs of tissue-cultured embryonic chick cardiac myocytes [9–12] and rat atrial myocytes [10]. Mechanical stretching has been suggested to increase the amplitude of  $\text{Ca}^{2+}$  transients by activating SACs, which, in turn, increases their  $\text{Ca}^{2+}$  permeability [12, 13].

Although the L-type  $\text{Ca}^{2+}$  channel is considered the main pathway of  $\text{Ca}^{2+}$  entry during an action potential (AP) in cardiomyocytes [14, 15], there are several studies showing that uniaxial stretching does not affect the L-type  $\text{Ca}^{2+}$  current ( $I_{\text{Ca,L}}$ ) in single cardiomyocytes [16–19]. However, in our previous studies, we observed inhibition of  $I_{\text{Ca,L}}$  during uniaxial stretching using a glass stylus [6, 8]. This inhibition was attributed to the intracellular accumulation of  $\text{Ca}^{2+}$  due to the  $\text{Ca}^{2+}$  influx through SACs. To date, no studies have been conducted that examined the dependence of the value of  $I_{\text{Ca,L}}$  on the degree of axial cell stretching. Although there may be no significant changes in  $I_{\text{Ca,L}}$  by uniaxial stretch in a voltage clamp experiment, extra  $\text{Ca}^{2+}$  may still enter the cell through L-type  $\text{Ca}^{2+}$  channels during prolongation in the depolarization phase of AP due to delayed voltage-dependent inactivation, which partly contributes to the increase in the amplitude of the  $\text{Ca}^{2+}$  transients [6, 20]. To examine the effects of cell stretching on L-type  $\text{Ca}^{2+}$  channels in rat ventricular myocytes, we investigated the operation of these channels under different degrees of dosed stretching.

In addition, to understand the function of operative SACs and  $\text{Ca}^{2+}$  channels, RNA reads encoding all existing channels in adult rat ventricular myocytes were examined. The data obtained showed the maximum number of

RNA reads for the  $\text{Ca}_v1.2$  channels, which exhibit additional mechanosensitive properties. Among mechanosensitive channels, we identified significant amounts of transcripts for transient receptor potential ion channels, including (melastatin) TRPM7, (canonical) TRPC1, and TRPM4.

## Materials and methods

### Animals

The experiments were conducted in compliance with the Guide for the Care and Use of Laboratory Animals (8th edition, 2011) published by the US National Institutes of Health, and the experimental protocol was approved by the Ethics Committee of the Russian National Research Medical University. Male outbred Wistar rats ( $n=34$ ) weighing between 220 and 270 g (10–12 weeks) were housed in a standard T4 cage in a 12:12 h light : dark cycle and given *ad libitum* access to food for four weeks prior to the start of the experiment.

### Solutions

$\text{Ca}^{2+}$ -free physiological salt solution ( $\text{Ca}^{2+}$ -free PSS) containing (in mM): 118 NaCl, 4 KCl, 1  $\text{MgCl}_2$ , 1.6  $\text{NaH}_2\text{PO}_4$ , 24  $\text{NaHCO}_3$ , 5 sodium pyruvate, 20 taurine, and 10 glucose, adjusted to pH 7.4 with NaOH (bubbled with carbogen 95%  $\text{O}_2$ +5%  $\text{CO}_2$ ). Enzyme medium containing:  $\text{Ca}^{2+}$ -free PSS supplemented with 10  $\mu\text{M}$   $\text{CaCl}_2$ , 0.2 mg  $\text{ml}^{-1}$  collagenase (Type II, Worthington, 225 U  $\text{mg}^{-1}$ ), and 1 mg  $\text{ml}^{-1}$  bovine serum albumin (Sigma). Before the actual experiments, cells were stored for at least 2 h in a modified Kraftbrühe (KB) medium, containing (mM): 50 L-glutamic acid, 30 KCl, 3  $\text{MgSO}_4 \times 7\text{H}_2\text{O}$ , 20 taurine, 10 glucose, 30  $\text{KH}_2\text{PO}_4$ , 0.5 EGTA, and 20 HEPES, adjusted to pH 7.3 with KOH [6]. The isolated cells were stored in KB medium for up to 8 h. Ventricular cardiomyocytes were perfused with a solution (37 °C) containing (mM): 150 NaCl, 5.4 KCl, 1.8  $\text{CaCl}_2$ , 1.2  $\text{MgCl}_2$ , 20 glucose, and 5 HEPES, at pH 7.4, adjusted with NaOH ( $\text{K}^+$  out solution). Internal pipette solution containing (mM): 140 KCl, 5  $\text{Na}_2\text{ATP}$ , 5  $\text{MgCl}_2$ , 0.01 EGTA and 10 Hepes/KOH at pH 7.3 ( $\text{K}^+$  in solution). Later in the text, this configuration is referred to as  $\text{K}^+$  in/ $\text{K}^+$  out solutions. In some experiments, we suppressed *inward rectifying*  $\text{K}^+$  currents by substituting  $\text{Cs}^+$  for extracellular  $\text{K}^+$  and reduced *outward rectifying*  $\text{K}^+$  currents by replacing  $\text{K}^+$  with  $\text{Cs}^+$  in the intracellular (electrode) solution. Below in the text, this configuration is referred to as  $\text{Cs}^+$  in/ $\text{Cs}^+$  out solutions. For this, in a perfusion solution, 5.4 mM KCl was replaced by 5.4 mM CsCl (extracellular  $\text{Cs}^+$  out solution), while in the patch pipette solution, 140 mM KCl was replaced by 140 mM CsCl (intracellular  $\text{Cs}^+$  in solution) [5]. With suppressed  $\text{K}^+$  currents, the peak L-type  $\text{Ca}^{2+}$  current can be approximated by subtracting the late current ( $I_l$ ) from the most negative current surge [21]. A

similar substitution was made to separate the effects of non-selective cation currents  $I_{ns}$  [5, 6].

#### Isolated cardiomyocyte preparation

We followed a modified version of the previously described cell isolation procedure [5, 6]. Male Wister rats were anesthetized with an intraperitoneal injection of 80 mg kg<sup>-1</sup> ketamine and 10 mg kg<sup>-1</sup> xylazine, with heparin (1000 U kg<sup>-1</sup>) added to the anesthetic solution to prevent blood coagulation in the coronary vessels of the excised heart. The chest was opened, and the heart was rapidly excised and attached to a Langendorff apparatus with a constant flow of 1 ml min<sup>-1</sup> at 37 °C to flush the coronary vessels in carbogen-bubbled Ca<sup>2+</sup>-free PSS for 5 min. After this initial perfusion, hearts were retrogradely perfused with the same PSS supplemented with Worthington type II collagenase (0.5 mg ml<sup>-1</sup>), 1 mg ml<sup>-1</sup> bovine serum albumin (Sigma), and 10 μM CaCl<sub>2</sub> for 18–20 min. The perfusate was continuously bubbled with carbogen (95% O<sub>2</sub>+5% CO<sub>2</sub>), and the temperature was equilibrated at 37 °C. The enzymes were then washed out with a modified KB medium [22], and the heart was disconnected from the perfusion system. The ventricles were then cut off, chopped, and gently triturated to release the cells into the KB medium. The resulting cell suspension was filtered and stored in KB medium at 22 °C prior to use.

#### mRNA isolation and purification

mRNA was isolated directly from cardiomyocytes using Oligo-dT25 Dyna beads® (Invitrogen). The mRNA-bound beads were washed in a Tris buffer solution containing lithium dodecyl sulfate (LiDS) or without LiDS (Buffer A: 10 mM TrisHCl (pH 7.5); 0.15 M LiCl; 1 mM EDTA; 0.1% LiDS; Buffer B: 10 mM TrisHCl (pH 7.5); 0.15 M LiCl; 1 mM EDTA). The beads were resuspended in RNase-free water (Sigma, Dorset, UK), and the mRNA was reverse transcribed using cloned AMV reverse transcriptase (Invitrogen). The resulting cDNA was stored at -80 °C until necessary.

#### RNA sequencing and analysis

The obtained libraries were analyzed for concentration, size distribution, and quality using a dsDNA high sensitivity kit (Invitrogen, Carlsbad, CA, USA) on a Qubit 4 fluorometer (Thermo Fisher Scientific, Inc., Dreieich, Germany) and a high sensitivity D5000 kit (Agilent, Santa Clara, CA, USA) on a 4200 TapeStation. Libraries were normalized according to their molarity, pooled, and then quantified with a library quantification kit for Illumina platforms (Roche, Basel, Switzerland) using a StepOnePlus qPCR machine (Thermo Fisher Scientific, Inc., Dreieich, Germany). The resulting pooled libraries were loaded at 350 pM with 1% PhiX on an S2 FlowCell and

sequenced in triplicate using a NovaSeq 6000 next-generation sequencer (Illumina, San Diego, CA, USA) with paired-end reads of 2×150 bp.

Raw FASTQ - sequenced reads were first assessed for quality using FastQC v0.11.5 (available online at <http://www.bioinformatics.babraham.ac.uk/projects/fastqc/>) [23]. The reads were then passed through Trimmomatic v0.36 [24] for quality trimming and adapter sequence removal. The surviving trimmed read pairs were then processed with Fastp [25] to remove poly-G tails and Novaseq/Nextseq-specific artifacts. Following the quality trimming, the reads were assessed again using FastQC. Post - QC and QT, the reads were aligned to the human reference genome GRCh38.p4 using HISAT2 [26] with default parameters, and the resulting SAM alignments were then converted to BAM format and coordinate sorted using SAM Tools v1.3.1 [27]. Finally, the sorted alignment files were analyzed with HTSeq-count v0.6.1p1 [28] using the options (-s no -t exon -I gene\_id) for raw count generation.

Unless otherwise stated, all experiments were performed with at least three replicates, and the data are represented as the mean ± standard error (SE).

#### Compounds

In certain experiments, nifedipine (Sigma-Aldrich), a specific blocker of the L-type Ca<sup>2+</sup> channel [29], was added to the bath solution at a concentration of 5–10 μM to assess the pharmacological specificity of the observed Ca<sup>2+</sup> currents [30, 31]. At these concentrations, nifedipine selectively blocks  $I_{Ca,L}$  without affecting the *T-type* Ca<sup>2+</sup> current ( $I_{Ca,T}$ ), the *fast* Na<sup>+</sup> current, the *delayed rectifier* current ( $I_K$ ), or the hyperpolarization-activated *inward* current [29]. Isoproterenol, a β-adrenergic stimulator, dose-dependently stimulated  $I_{Ca,L}$  in isolated cardiac myocytes, reaching a plateau at 100 nM. The effect of isoproterenol (Sigma-Aldrich) (20 nM) on the peak current amplitudes of  $I_{Ca,L}$  at 0 mV was considered a test of the quality of isolated cells. Gadolinium (Gd<sup>3+</sup>) (Sigma-Aldrich), known as a non-specific blocker of mechanically gated channels in the  $I_{SAC}$  (current through stretch activated channels) [5, 6], was added to the PSS (5 μM GdCl<sub>3</sub>), BAPTA (Tocris), and 1,2-bis(2-aminophenoxy)ethane-N,N,N',N'-tetraacetic acid.

#### Mechanical stretch of the ventricular myocytes

The mechanical stimulation method used in this study has previously been described in detail. Here, we only report the peculiarities relevant to this study. After whole-cell access with the patch pipette (P), a fire-polished glass stylus (S) was attached to the membrane [5, 6, 22, 32]. When the stylus was newly polished and the surface membrane was clean, the attachment was successful in approximately 70% of the attempts. The stylus was

then lifted 2  $\mu\text{m}$  to prevent ‘scratching’ of the lower cell surface on the coverslip during the stretch. A motorized micromanipulator (MP 285, Sutter, Novato, Calif., USA, accuracy 0.2  $\mu\text{m}$ ) increased the S-P distance stepwise by up to 12  $\mu\text{m}$ , with P being the fixed point [5, 22]. Stretch and release of stretch could be repeated 3–4 times with the same cell, on average. Our method was shown to stretch the cell surface locally, while the membrane in the line between P and S was stretched as expected (approximately 80% of the entire membrane surface remains unaffected) [5, 22]. The effect of mechanical stretching on the sarcomere pattern was imaged by a slow-scan CCD camera (Princeton Instruments, Trenton, N.J., USA) and evaluated by Meta Morph software (Universal Imaging, West Chester, PA, USA). S and P were positioned 40  $\mu\text{m}$  apart before attaching them to the cell. Cell stretching by 4  $\mu\text{m}$  (increasing the S - P distance) increased local stretching by approximately 6%, by 6  $\mu\text{m}$  about 10%, by 8  $\mu\text{m}$  about 14%, and by 10  $\mu\text{m}$  about 18%. These values were less than expected but close to those previously obtained in isolated mouse cardiomyocytes. Presumably, the extent of local stretch decays from the cell surface to the interior of the cell, where the optical focus was set [6, 22].

To investigate the effect of cell stretch at 4, 6, 8, and 10  $\mu\text{m}$  on  $I_{\text{Ca,L}}$  values, measurements were taken. A standard elongation of 6  $\mu\text{m}$  was used to study  $I_{\text{Ca,L}}$  on the background of cell elongation under the action of various compounds.

### Whole-cell patch-clamp

A total of 113 cells ( $n=113$ ) were used in the experiments. Whole-cell patch-clamp recordings of  $K^+$ ,  $\text{Ca}^{2+}$ , and non-selective ( $I_{\text{ns}}$ ) currents were obtained using an Axopatch 200B amplifier and pClamp 10 software (Molecular Devices, San Jose, CA, USA). The data were filtered at 2 kHz, sampled at 5 kHz, and analyzed using the same software. Myocytes were superfused in a small recording chamber (RC-26; Warner Instrument Corp., Brunswick, CT, USA) with a volume of 150  $\mu\text{l}$ , which was mounted on an inverted microscope.

The borosilicate glass patch-clamp electrodes had tip resistances ranging from 1.5 to 2.5  $\text{M}\Omega$  when filled. Cell access was obtained by rupturing the patch after seal formation. Pulses of 140 ms and 350 ms were applied at 1 Hz, starting from a holding potential ( $V_{\text{hp}}$ ) of  $-45$  mV, which caused the inactivation of tetrodotoxin (TTX)-sensitive  $\text{Na}^+$  currents. To evaluate membrane capacitance and access resistance, currents in response to trains of short (5 mV) pulses applied at  $-45$  mV were taken without compensation for capacitive and leak currents. Cells with similar geometry were selected based on their length and diameter (control rat ventricular cardiomyocytes had an average diameter of  $25\pm 6$   $\mu\text{m}$ ),

and, on average, had a membrane capacitance of  $150\pm 16$  pF ( $n=16$ ) and an input resistance of  $58\pm 5$   $\text{M}\Omega$  (in 16 representative cells). Glass tools were adjusted to the same 40  $\mu\text{m}$  S -P distance before the application of stretch to minimize the effect of differences in the size of the stretched membrane. Since the area of mechanical stretching was small and unknown, we did not divide the stretch-induced currents by the entire membrane capacitance.

Currents through L-type  $\text{Ca}^{2+}$  channels, membrane currents at the end of the pulse (late current:  $I_{\text{L}}$ ), and other currents were plotted as functions of their respective clamp step potentials. The seal resistance remained constant, i.e. it was  $1.5\pm 0.3$   $\text{G}\Omega$  before and  $1.4\pm 0.4$   $\text{G}\Omega$  during the stretch. Similarly, access resistance and membrane capacitance remained unaffected, indicating that the stretch-induced inward current was due to the activation of an ionic current rather than leakage around the seal. The zero current potential ( $V_0$ ) for  $I_{\text{L}}$  was determined by the intercept of the resulting  $I/V$  curve with the voltage axis and corresponded to the resting membrane potential of a non-clamped cell (between  $-70$  and  $-80$  mV). Online records of net membrane current were carried out at  $V_{\text{hp}}=-45$  mV (time course) [6, 22, 33].

Typically, the measurements lasted approximately 30 min, during which time the access resistance and capacitive current remained stable. To obtain the current-voltage relations ( $I/V$  curves), a series of 20 pulses of 140 ms (or 350 ms) duration were applied, starting from  $V_{\text{hp}}=-45$  mV.

Freshly isolated brick-like cardiomyocytes can attach to the glass bottom in two different positions: edgewise, staying on the narrow side, and broadwise, staying on the broad side [34]. However, the response to stretching is identical in cardiomyocytes occupying both positions (edgewise and broadwise). On the other hand, the response to compression differs depending on the cell's position [34, 35]. For our experiments, we selected cells that stayed on the narrow side (edgewise) and had similar sizes.

In this study,  $I_{\text{Ca,L}}$  recordings are presented in both absolute values (e.g., pA) and normalized form (e.g., pA/pF). However, changes in  $I_{\text{Ca,L}}$  in response to cell stretching or treatment with compounds are presented as the difference between  $I_{\text{Ca,L}}$  under control conditions and that under stretching or treatment conditions.

### Statistics

Values are presented as means  $\pm$  SD. To determine significant differences, we used Analysis of Variance (ANOVA) with the Bonferroni test as a post-hoc analysis. For cases where multiple factors were evaluated, a two-way ANOVA was performed. Statistical significance was set at  $p<0.05$ .



## Results

### The levels of the channel's gene expression

In this study, we used RNA-seq to measure the expression levels of various genes in freshly isolated rat ventricular cardiomyocytes. Our analysis revealed the presence of RNA reads encoding different ion channels, as summarized in Table 1 [36–92], and illustrated in Fig. 1. Specifically, we found that  $\text{Na}_v$  channel transcripts were expressed in these cells, with  $\text{Na}_v1.5$  showing the highest number of RNA reads ( $3654.4 \pm 581.2$ ), followed by  $\text{Na}_v1.1$  (only  $179 \pm 30$ ), [81, 82]. The expression of other  $\text{Na}_v$  channels was minimal. Importantly, previous research has shown that  $\text{Na}_v1.5$  exhibits mechanosensitivity [81, 82], which may have physiological implications for the function of rat ventricular cardiomyocytes.

Our analysis revealed the presence of three  $\text{Ca}_v$  subfamilies:  $\text{Ca}_v1.2$ ,  $\text{Ca}_v1.3$ , and  $\text{Ca}_v1.1$ , as shown in Fig. 1. Of these, the  $\text{Ca}_v1.2$  channels had the highest number of RNA reads ( $1336.66 \pm 71.8$ ), with the transcripts of the other  $\text{Ca}_v$  channels being an order of magnitude smaller. In particular, previous studies have shown that  $\text{Ca}_v1.2$  and  $\text{Ca}_v1.3$  both exhibit mechanosensitivity [84] (Table 1; Fig. 1). When considering the L-type  $\text{Ca}_v$  channels, which are responsible for the L-type  $\text{Ca}^{2+}$  current, we found that the  $\text{Ca}_v1.2$  transcripts were significantly more abundant than the  $\text{Ca}_v1.3$  transcripts ( $17.33 \pm 2.03$ ), while the number of  $\text{Ca}_v1.1$  transcripts was very low (Table 1). Based on these results, we conclude that  $\text{Ca}_v1.2$  is likely the primary channel that contributes to the L-type  $\text{Ca}^{2+}$  current in rat ventricular cardiomyocytes and that  $\text{Ca}_v1.3$  and  $\text{Ca}_v1.1$  can be neglected. This finding is consistent with previous research indicating that  $\text{Ca}_v1.2$  channels are the main contributors to the L-type  $\text{Ca}^{2+}$  current [84].

Among the multitude of  $\text{K}_v$  channel transcripts (Fig. 1), the  $\text{K}_v7.1$  or  $\text{KCNQ1}$  channel had the highest number of RNA reads ( $821.00 \pm 77.20$ ), consistent with previous studies showing its response to membrane stretch [88] and hypo-osmotic swelling [88, 89] (Table 1). The  $\text{K}_v1.2$  channel, which has also been shown to exhibit mechanosensitivity [67], was present in smaller quantities with  $212.00 \pm 10.02$  RNA reads (Table 1; Fig. 1). In particular, the number of  $\text{K}_v1.2$  transcripts was 3.5 times less than that of the predominant  $\text{K}_v7.1$  (Fig. 1).

Among  $\text{K}_2\text{P}$  channels,  $\text{TREK-1/K}_2\text{P2.1}$  had the highest number of RNA reads ( $153.00 \pm 11.93$ ) compared to others, consistent with its established mechanosensitivity [75–77].  $\text{TRAAK/K}_2\text{P4.1}$  channels also exhibit mechanosensitivity [76, 93], although the number of detected RNA reads was very small ( $0.66 \pm 0.33$ ) (Table 1; Fig. 1). Interestingly, transcripts of the mechanosensitive channels  $\text{TREK-2/K}_2\text{P10.1}$ , which are expressed in the atrial and ventricular cells of human and murine hearts [76], were not detected in our isolated rat ventricular myocytes.

The RNA-seq technique revealed the presence of several Kir channel transcripts (Fig. 1) in freshly isolated rat ventricular cardiomyocytes. Among them, Kir6.2 ( $1240.66 \pm 57.1$ ) was detected in the highest abundance and demonstrated mechanosensitivity only when associated with the sulfonylurea receptor 2 A (SUR2A) subunit [91] (Table 1; Fig. 1). Additionally, RNA reads were found for Kir6.1 channels ( $82.66 \pm 6.49$ ), which are also mechanosensitive [92]. However, unlike mouse ventricular cardiomyocytes, where Kir2.3 channels have been shown to be mechanosensitive [22], we did not detect any RNA reads for Kir2.3 channels in rat ventricular cardiomyocytes.

We identified three types of stretch-activated  $\text{K}_{\text{Ca}}$  (SAKCA), or  $\text{BK}_{\text{Ca}}$  channels, that exhibit mechanosensitivity [78]: calcium-activated potassium channel subunit beta-2 ( $\text{KCNMB2}$ ) ( $6.6 \pm 0.9$ ),  $\text{KCNMB4}$  ( $2.7 \pm 0.9$ ), and  $\text{KCNMB1}$  ( $0.3 \pm 0.3$ ) (Table 1; Fig. 1). Although ATP-sensitive potassium channels ( $\text{K}_{\text{ATP}}$ ) also exhibit mechanosensitivity in rats [41, 80], we did not investigate their presence in our study. Likewise, we did not analyze the expression of  $\text{Kv7}$  ( $\text{KCNQ}$ ) channels [88–90].

We observed several transcripts for nonselective cation TRP channels, many of which are known to be mechanically gated (listed in descending order of RNA reads). In particular, mechanosensitive  $\text{TRPM7}$  ( $333.5 \pm 31.5$ ) [36–39, 94],  $\text{TRPC1}$  ( $146.66 \pm 6.96$ ) [40, 42, 43],  $\text{TRPM4}$  ( $179.66 \pm 5.93$ ) [44–47, 95],  $\text{TRPV2}$  ( $21.66 \pm 2.03$ ) [48, 49],  $\text{TRPC3}$  ( $5.0 \pm 3.0$ ) [50–55, 96],  $\text{TRPV4}$  ( $5.5 \pm 0.5$ ) [56–58],  $\text{TRPV1}$  ( $2.00 \pm 0.58$ ) [59, 60],  $\text{TRPM3}$  ( $1.3 \pm 0.9$ ) [61],  $\text{TRPC5}$  ( $1.3 \pm 0.9$ ) [62, 97],  $\text{TRPA1}$  ( $1.0 \pm 0.9$ ) [63–65], and  $\text{TRPC6}$  ( $1.0 \pm 1.0$ ) [22, 47, 66, 67, 97] were among the most abundant.

We also identified two additional stretch-activated channels, Piezo 1 ( $145.33 \pm 8.01$ ) [71–73, 98, 99], and Piezo 2 ( $6.0 \pm 2.0$ ) [73, 74], that were present in the ventricular cardiomyocytes of rats.

The data presented here and below reveal an intriguing observation: While many ion channels have been studied in terms of their response to membrane stretch, only a few have been thoroughly investigated. However, among those that have been studied, all demonstrate a certain degree of mechanosensitivity. On the basis of this, it is plausible to speculate that mechanosensitivity is a ubiquitous characteristic of ion channels and that all channels, irrespective of their gating mechanism, should respond to membrane stretch and tension.

### Definition and analysis of L-type $\text{Ca}^{2+}$ current

In this study, two methods were used to estimate the current through L-type  $\text{Ca}^{2+}$  channels ( $I_{\text{Ca,L}}$ ) in  $\text{K}^+_{\text{in}}/\text{K}^+_{\text{out}}$  solutions. The first method involved evaluating the time course of  $I_{\text{Ca,L}}$  by subtracting the late current at the end of the 140 ms pulse from the negative peak current

**Table 1** Identified mechanically gated channels and channels with mechanosensitivity in our experiments and in the literature

Ion channels	Species	Material for analysis	Number of reads mapped	Num-ber of tests (n)	Known data Species	Location	Mechanosensitivity
<b>Mechanically gated channels:</b>							
<i>Non-selective cation channels</i>							
TRPM7	Rat	Isolated ventricular myocytes	333.5 ± 31.5	3	Pig and Human Human TRPM7 Human TRPM7	Atrial tissues [36] TRPM7 channel expressed in HeLa cells TRPM7 channel expressed in HEK293T cells	The authors did not investigate TRPM7 is a stretch-activated channel [37]. TRPM7 single channels are directly activated by stretch [38]. TRPM7 is directly activated by shear stress [39]
TRPC1	Rat	Isolated ventricular myocytes	146.66 ± 6.96	3	Human Rat	Heart [40] Atrial myocyte, ventricular myocyte, Purkinje cells	The authors did not investigate TRPC1 is a stretch-activated channel [40, 41]
TRPM4	Rat	Isolated ventricular myocytes	179.66 ± 5.93	3	Human TRPC1 Human TRPC1 Human TRPC1	Human TRPC1 transfected into CHO-K1 cells TRPC1 channel expressed in oocytes <i>Xenopus laevis</i> Human TRPC1 transfected into CHO-K1 cells	TRPC1 mediate stretch-activated currents [42] TRPC1 is a stretch-activated channel [43] TRPC1 is a mechanosensitive channel [43] The authors did not investigate
TRPV2	Rat	Isolated ventricular myocytes	21.66 ± 2.03	3	Rat Human Rat	Freshly isolated cardiomyocytes from the left ventricles [45] Human TRPM4 transfected into HEK293 cells [46] Cerebral artery myocytes [47]	The authors did not investigate TRPM4 is a mechanosensitive channel [46, 47].
TRPC3	Rat	Isolated ventricular myocytes	5.00 ± 3.00	3	Mice Mice Human Mice Rat Mice Mice Mice Canis	Freshly dispersed vascular smooth muscle aortic myocytes Heart [40] Ventricular myocytes [50] Ventricular myocytes [51] Ventricular myocytes [52] Ventricular myocytes Cardiac atrial fibroblasts TRPC3 expressed in NDC cells or CHO	The authors did not investigate TRPV2 is a mechanosensitive channel [49]. The authors did not investigate TRPC3 is a stretch-activated channel [53] TRPC3 is a stretch-activated channel [54] TRPC3 is a stretch-activated channel [55]

**Table 1** (continued)

Ion channels	Species	Material for analysis	Number of reads mapped	Number of tests (n)	Known data Species	Location	Mechanosensitivity
TRPV4	Rat	Isolated ventricular myocytes	5.5 ± 0.50	3	Neonatal rat Rat TRPV4 Human Murine TRPV4	Cultured ventricular myocytes TRPV4 channel expressed in oocytes <i>Xenopus laevis</i> Heart [40] The TRPV4 channel expressed in vitro in Chinese hamster ovary cells	TRPV4 is a stretch-activated channel [56] TRPV4 is a stretch-activated channel [57]. The authors did not investigate TRPV4 is a mechanosensitive channels [58].
TRPV1	Rat	Isolated ventricular myocytes	2.00 ± 0.58	3	Rat	Kidney. Cloned from the rat kidney	TRPV1 is a mechanosensitive channel (initially named "stretch-inactivated channel"), [59].
TRPM3	Rat	Isolated ventricular myocytes	1.33 ± 0.88	3	Mice Human, bovine, mice	Bladder urothelium TRPM3-expressing HEK-293 cells (Expression in bovine and human kidney; in mouse and human brain).	TRPV1A is a mechanosensitive channel [60]. TRPM3 is a mechanosensitive channel [61]
TRPC5	Rat	Isolated ventricular myocytes	1.33 ± 0.88	3	Human Murine TRPC5	Heart [40] TRPC5 channel expressed in HEK-293 cells	The authors did not investigate TRPC5 is a stretch-activated channel [62]
TRPA1	Rat	Isolated ventricular myocytes	1.0 ± 0.9	3	Drosophila Mice	Heart [63] Inner ear hair cells <i>Caenorhabditis elegans</i>	TRPA1 is a mechanosensitive channel [63] TRPA1 is a mechanosensitive channel [64] TRPA1 is a mechanosensitive channel [65]
TRPC6	Rat	Isolated ventricular myocytes	1.0 ± 1.0	3	Human Mice TRPC6 Cerebral artery Heart Mice	Heart [40] Isolated ventricular myocytes HEK-293 cells were transfected with the TRPC6 vector Myocytes Ventricular myocyte Vascular smooth muscle cells	The authors did not investigate TRPC6 is a stretch-activated channel [22] TRPC6 is a mechanosensitive channel [66] TRPC6 is a mechanosensitive channel [47] TRPC6 is a mechanosensitive ion channel [68]
PKD1 (Polycys-tin-1, TRPP1)	Rat	Isolated ventricular myocytes	267.33 ± 17.9	3	Heart	Ventricular myocyte	TRPP1 (PKD1) is a mechanosensitive ion channel [69, 70]
PKD2 (Polycys-tin2, TRPP2)	Rat	Isolated ventricular myocytes	191.66 ± 35.09	3	Heart	Ventricular myocyte	TRPP2 (PKD2) is a mechanosensitive ion channel [69, 70]
Piezo 1	Rat	Isolated ventricular myocytes	145.33 ± 8.01	3	Human Piezo1 Adult human Rat	Piezo1 transfected into HEK-293 cells Adult human ventricular cardiomyocyte AC16 Piezo1 channels were natively expressed in dorsal root ganglia tissue. Piezo2 channels were natively expressed in rat dorsal root ganglia tissue.	Piezo1 is a mechanosensitive channel [71] Piezo1 is a stretch-activated channel [72] Piezo1 is a mechanosensitive channel [73]
Piezo 2	Rat	Isolated ventricular myocytes	6.0 ± 2.0	3	Rat Mice	Piezo2 channels were natively expressed in rat dorsal root ganglia tissue. Vagal sensory nerves	Piezo2 is a mechanosensitive channel [73] Piezo2 is a mechanosensitive channel [74]

**Mechanically gated channels:**  
MGCh<sub>k</sub>

**Table 1** (continued)

Ion channels	Species	Material for analysis	Number of reads mapped	Number of tests (n)	Known data Species	Location	Mechanosensitivity
TREK-1/ $K_{sp2.1}$	Rat	Isolated ventricular myocytes	153,00 ± 11,93	3	Rat	Isolated ventricular myocyte Ventricular myocyte	TREK-1 is a stretch-activated channel [75] TREK-1 is a mechanosensitive channel [75] TREK-1 ( $K_{sp2.1}$ ) is a mechanosensitive channel [76]
TRAAK/ $K_{sp4.1}$	Rat	Isolated ventricular myocytes	0.66 ± 0.33	3	Murine TREK-1 Human and murine heart TRAAK/ $K_{sp4.1}$	TREK-1 transfected into COS cells Atrial and ventricular tissue TRAAK transfected into COS cells	TREK-1 is a mechano-gated $K^+$ channel [77] TRAAK ( $K_{sp4.1}$ ) is a stretch-activated channel [76] TRAAK ( $K_{sp4.1}$ ) is a stretch-sensitive $K_{sp}$ channel [76] Stretch-activated cardiac $K_{sp}$ channels [76]
TREK-2/ $K_{sp10.1}$	Rat	Isolated ventricular myocytes	0	3	Human, Mice	Heart: atrial and ventricle	SAKCA or $BK_{Ca}$ Different Types: KCNMB2 KCNMB4 KCNMB1 KCNMB2 ( $BK_{Ca}$ )
KCNMB4	Rat	Isolated ventricular myocytes	6.66 ± 0.88	3	Chick SAKCA	Ventricular myocyte SAKCA cloned from the heart	SAKCA is a mechanosensitive channel [78] SAKCA is a mechanosensitive channel [79]
KCNMB4 ( $BK_{Ca}$ )	Rat	Isolated ventricular myocytes	2.66 ± 0.88	3			The authors did not investigate
KCNMB1 ( $BK_{Ca}$ )	Rat	Isolated ventricular myocytes	0.33 ± 0.33	3			
$K_{ATP}$	Neonatal and adult rat Rat				Neonatal and adult rat Rat	Atrial myocyte Ventricular myocytes	$K_{ATP}$ is a mechanosensitive channels [80] $K_{ATP}$ are mechanosensitive channels [41]
<b>Voltage-gated channels</b>							
with mechano-sensitivity $VGCh_{MS}$							
$Na_v1.5$	Rat	Isolated ventricular myocytes	3158.0 ± 405.7	3	Human heart $Na_v1.5$	$Na_v1.5$ channel expressed in HEK 293 cells $Na_v1.5$ channel expressed in <i>Xenopus laevis</i> oocytes	$Na_v1.5$ is a mechanosensitive channel [81] $Na_v1.5$ is mechanosensitive channel [82]
$Na_v1.6$	Rat	Isolated ventricular myocytes	1.0 ± 1.0	3	Mouse $Na_v1.6$	$Na_v1.6$ channel expressed in <i>Xenopus laevis</i> oocytes	$Na_v1.6$ is mechanosensitive channel [83]
$Ca_v1.2$ L-type	Rat	Isolated ventricular myocytes	1336.66 ± 71.8	3	$Ca_v1.2$ subunits	$Ca_v1.2$ subunits transfected into HEK-293	Cloned $Ca_v1.2$ channel exhibits mechanosensitive behavior similar to the native channel [84]
$Ca_v1.3$ L-type	Rat	Isolated ventricular myocytes	17.33 ± 2.03	3	Mice	Inner hair cells (IHCs)	$Ca_v1.3$ is mechanosensitive channel [85]



**Table 1** (continued)

Ion channels	Species	Material for analysis	Number of reads of mapped	Num-ber of tests (n)	Known data Species	Location	Mechanosensitivity
Ca <sub>v</sub> 1.1 L-type	Rat	Isolated ventricular myocytes	0.33 ± 0.33	3		The authors did not investigate	The authors did not investigate
Ca <sub>v</sub> 2.2 N-type	Rat	Isolated ventricular myocytes	0	3	Human	Human embryonic kidney T-antigen-transformed (HEK-293T) cells	Patch-stretch whole cell (1) and whole cell inflation (2) [86]
K <sub>v</sub> 1.2	Rat	Isolated ventricular myocytes	212.00 ± 10.02	3	K <sub>v</sub> 1.2 channels		K <sub>v</sub> 1.2 is a mechanosensitive channel [67]
K <sub>v</sub> 1.5	Rat	Isolated ventricular myocytes	30.66 ± 1.67	3	K <sub>v</sub> 1.5 channel	K <sub>v</sub> 1.5 channel expressed in <i>Xenopus</i> oocytes	Stretch by suction (negative pressure) via patch pipette [87]
K <sub>v</sub> 3.2	Rat	Isolated ventricular myocytes	0.33 ± 0.33	3	K <sub>v</sub> 3.2 channels	K <sub>v</sub> 3.2 channel expressed in <i>Xenopus</i> oocytes	Stretch by suction (negative pressure) via patch pipette [87]
KCNQ					Chick	Ventricular myocytes	KCNQ channel responds to membrane stretch [67]
K <sub>v</sub> 7.1 /KCNQ1	Rat	Isolated ventricular myocytes	821.00 ± 77.20	3	KCNQ1/ K <sub>v</sub> 7.1 channel	K <sub>v</sub> 7.1 channel expressed in <i>Xenopus</i> oocytes	KCNQ1 channel responds to membrane stretch [88]
					KCNQ1/ K <sub>v</sub> 7.1 channel	K <sub>v</sub> 7.1 channel expressed in <i>Xenopus laevis</i> oocytes	KCNQ1 channel responds to hypo-osmotic swelling. Voltage clamp (two-electrode) [89]
					KCNQ1/ K <sub>v</sub> 7.1 channel	K <sub>v</sub> 7.1 channel in CHO cells	Hypotonic swelling. Patch-clamp studies [90]
<b>Inward rectifier K<sup>+</sup>-channels (K<sub>ir</sub>) with mechano-sensitivity</b>							
K <sub>ir</sub> 6.2	Rat	Isolated ventricular myocytes	1240.66 ± 57.1	3	Human Kir6.2	Human Kir6.2 transfected into HEK293T	Kir6.2 is a mechanosensitive only with SUR2A subunit [91]
K <sub>ir</sub> 6.1	Rat	Isolated ventricular myocytes	82.66 ± 6.49	3	K <sub>ir</sub> 6.1	Expression of Kir6.1 was analyzed in human valve interstitial cells (VIC).	Kir6.1 is a mechanosensitive channel [92]
Kir2.3	Rat	Isolated ventricular myocytes	0	3	Mice	Ventricular myocytes	Kir2.3 is a mechanosensitive channel [22]

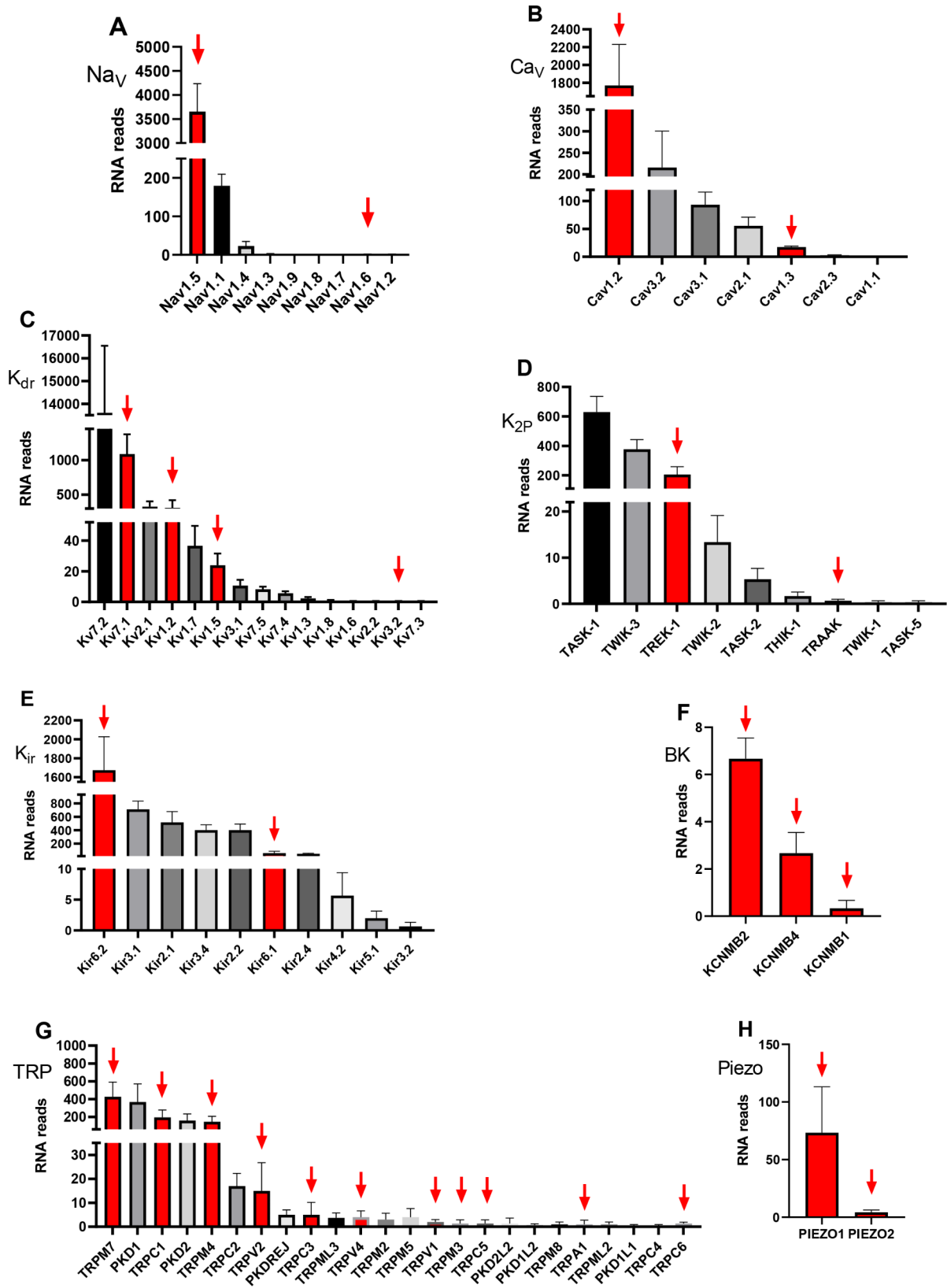


**Fig. 1** Relative abundance of ion channels encoding different channel genes in adult rat ventricular cardiomyocytes. Bars represent the mean  $\pm$  SEM (n = 10). Red columns and red arrows indicate mechanosensitive channels, while black and gray columns indicate all the rest

(Fig. 2A). The second method involved determining the current-voltage ( $I/V$ ) relationship for  $I_{Ca,L}$  by subtracting the current at the same potential in the presence of 5 or 10  $\mu\text{M}$  nifedipine from the maximum point of the negative peak current (Fig. 2B). The value of  $I_L$  at 0 mV was almost equal to the current in the presence of nifedipine (Fig. 2A). The negative peak current at 0 mV in control conditions (blue track) and in the presence of 10  $\mu\text{M}$  nifedipine (red track), which selectively blocks L-type  $\text{Ca}^{2+}$  channels, was used to estimate  $I_{Ca,L}$ .  $I_{Ca,L}$  was calculated by taking the difference between the negative peak current and the current in the presence of nifedipine (or by subtracting the late current at the end of the 140 ms or 350 ms pulse at a frequency of 1 Hz). Since the  $I/V$  relation of  $I_L$  in control (green triangles) completely coincides with the  $I/V$  relation for  $I_{Ca,L}$  in the presence of nifedipine (red circles) in the range from  $-80$  mV to  $+50$  mV (Fig. 2B), the calculation method presented in previous study for  $\text{K}^+_{in}/\text{K}^+_{out}$  solutions was applied [21], whereas  $I_{Ca,L}$  was estimated as the difference between the negative current at  $-10$  mV (blue circle) and either the current in the presence of nifedipine at  $-10$  mV (red circle) or the late current at  $-10$  mV in control (green triangles) (Fig. 2B).

It should be noted that in  $\text{K}^+_{in}/\text{K}^+_{out}$  solutions, the positive peak on the  $I/V$  relation for  $I_{Ca,L}$  between  $-30$  and  $-70$  mV (Fig. 2B: blue circles) is associated with the positive currents in response to voltage steps in this potential range and was first demonstrated by Josephson and Sperelakis (1982), [100]. However, not all subsequent studies on  $I_{Ca,L}$  took this positive peak into account.

Figure 2 C shows that in  $\text{Cs}^+_{in}/\text{Cs}^+_{out}$  solutions, the negative peak current at 0 mV in control conditions (blue track) and in the presence of 10  $\mu\text{M}$  nifedipine (red track) were used to estimate  $I_{Ca,L}$  by taking the difference between the peak current and the current in the presence of nifedipine or the late current at the end of the pulse. Figure 2D shows the  $I/V$  relations for  $I_{Ca,L}$  in control conditions (blue circles) and in the presence of nifedipine (red circles). In this case,  $I_{Ca,L}$  was calculated as the difference between the negative current (blue circles) and the current in the presence of nifedipine (red circles) or when the current equals 0 nA. The  $I/V$  relations for  $I_L$  measured at the end of the pulse are shown under control conditions (blue triangles) and in the presence of nifedipine (red triangles). Our experiments used an internal pipette solution containing 0.01 mM EGTA, and under these conditions, we measured the  $I_{Ca,L}$  value when cells were stretched by 4, 6, 8, and 10  $\mu\text{m}$ . Previous studies have shown that the reduction of  $I_{Ca,L}$ , even by a stretch of 10  $\mu\text{m}$ , was no longer observed when the cells were pre-dialyzed with 5 mM BAPTA, i.e., control  $I_{Ca,L}$  and  $I_{Ca,L}$  during stretch superimposed [6]. To study  $I_{Ca,L}$  in the context of cell elongation under the action of

various compounds, a standard elongation of 6  $\mu\text{m}$  was used in this study.

As demonstrated earlier in  $\text{K}^+_{in}/\text{K}^+_{out}$  solutions, the late current ( $I_L$ ) at the end of the pulse reflects the cell's response to stretching. Stretch-induced changes in  $I_L$  exhibit an outward rectifying voltage dependence with a reversal potential ( $E_{rev}$ ) of  $-16$  mV [5, 6]. To calculate stretch-induced current ( $\Delta^S I_L$ ), we take the difference between the control current values ( $^C I_L$ ) and the current values in the presence of cell stretching ( $^S I_L$ ) at  $-45$  or  $-80$  mV ( $\Delta^S I_{L(-45)}$  and  $\Delta^S I_{L(-80)}$ ) [5].

In our earlier work conducted on isolated mouse ventricular cardiomyocytes [5, 6], as well as in studies by our colleagues on the same cells [22], it was found that in  $\text{K}^+_{in}/\text{K}^+_{out}$  solutions, the net current was composed of  $I_{ns}$  (current through stretch-activated non-selective cation channels),  $I_{KI}$  (inwardly rectifying potassium current), and  $I_o$  (presumably the sum of several outwardly rectifying currents, such as  $\text{K}^+$  currents through TREK channels [76, 77] or the outwardly rectifying canonical transient receptor potential-6 (TRPC6) channels [66]). Cell stretch can modify net membrane currents ( $\Delta^S I_L$ ) by modulating both  $\text{K}^+$  and  $I_{ns}$  currents [5]. However, our present studies investigating the RNA transcripts of ion channels and their mechanosensitivity reveal significant differences in the channel spectrum of ventricular cardiomyocytes in adult rats (see below).

To distinguish the effects on  $I_{ns}$ , we used two methods: first, we eliminated inward rectifying  $\text{K}^+$  currents by substituting extracellular  $\text{K}^+$  with  $\text{Cs}^+$  and second, we decreased outward rectifying  $\text{K}^+$  currents by replacing intracellular  $\text{K}^+$  with  $\text{Cs}^+$ . In this case, the current through stretch-activated channels ( $I_{SAC}$ ) was calculated as the difference between the control current values ( $^C I_{ns}$ ) and the current values on the background of cell stretching ( $^S I_{ns}$ ) at  $-45$  or  $-80$  mV ( $I_{SAC(-45)}$  and  $I_{SAC(-80)}$ ). We used the same approach to measure the differential current in response to specific compounds ( $\Delta I_X$ ) (where "X" represents the compound) at  $-45$  or  $-80$  mV [5, 6].

Under our experimental conditions, isolated cardiomyocytes maintained their fundamental properties, as demonstrated by the significant increase in  $I_{Ca,L}$  peak current amplitudes at 0 mV in response to 20 nM isoproterenol in  $\text{K}^+_{in}/\text{K}^+_{out}$  and  $\text{Cs}^+_{in}/\text{Cs}^+_{out}$  solutions (not shown), which is consistent with previous literature reports for this compound [101].

#### Local stretch increased net currents $I_L$ and decreased $I_{Ca,L}$ in $\text{K}^+_{in}/\text{K}^+_{out}$ solutions (time-course and voltage-dependence)

Figure 3A.1 illustrates the effect of a 6  $\mu\text{m}$  cell stretch on time-dependent net membrane currents in  $\text{K}^+_{in}/\text{K}^+_{out}$  solutions. At control, the registered holding current (the current at  $V_{hp} = -45$  mV ( $I_{hc}$ )) was  $+0.44$  nA (label

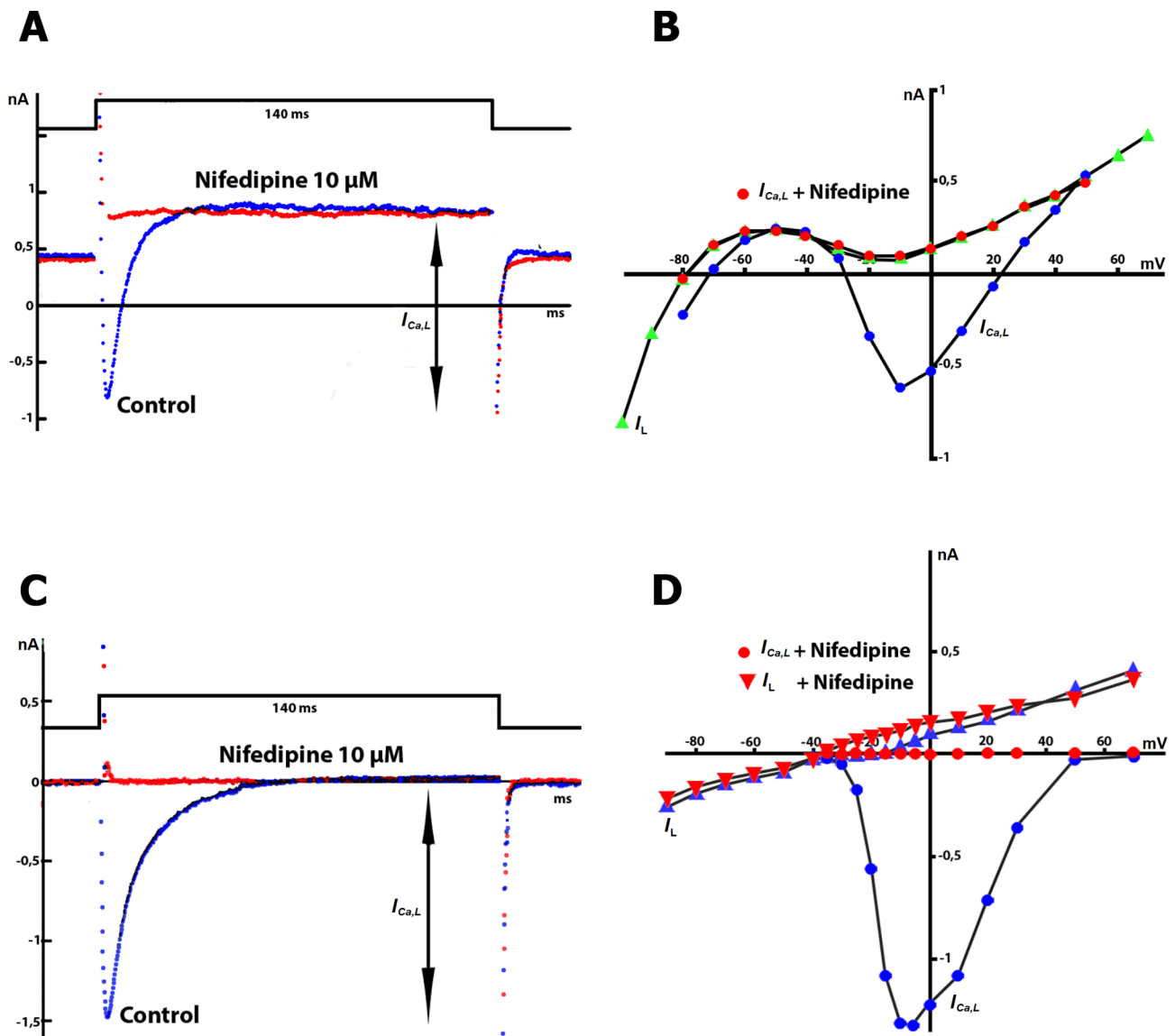


**Fig. 2** Evaluation of  $I_{Ca,L}$  and  $I_{hs}$  in  $K^+_{in}/K^+_{out}$  and  $Cs^+_{in}/Cs^+_{out}$  solutions. The membrane potential ( $V_m$ ) was maintained at  $V_{hp} = -45$  mV. **A:** Raw recordings of  $I_L$  and  $I_{Ca,L}$  (blue trace) and recordings in the presence of nifedipine (red trace) in  $K^+_{in}/K^+_{out}$  solutions. **B:** Current-voltage ( $I/V$ ) relationships for  $I_L$  (green triangles) and peak  $I_{Ca,L}$  (blue circles) under control conditions and in the presence of nifedipine (red circles). **C:** Raw recordings of  $I_L$  and  $I_{Ca,L}$  (blue trace) and recordings in the presence of nifedipine (red trace) in  $Cs^+_{in}/Cs^+_{out}$  solutions, where  $K^+$  currents are suppressed. **D:**  $I/V$  curves for  $I_L$  (blue triangles) and  $I_{Ca,L}$  (blue circles) under control conditions and in the presence of nifedipine (red circles)

C, Fig. 3A.1), and stretch changed this current ( $S_{I_{hc}}$ ) to +0.27 nA (label S, Fig. 3A1). The stretch-induced difference of the holding current  $\Delta^S I_{hc}$  was (-) 0.17 nA ((-)  $0.19 \pm 0.01$  nA,  $n=14$ ) at  $-45$  mV. The minus sign (-) emphasizes that cell stretch leads to more negative values of the initial net holding current at the level of  $V_{hp} = -45$  mV. The pulse to 0 mV induced the  $L$ -type  $Ca^{2+}$  current ( $I_{Ca,L}$ ) that activated and inactivated over time. The stretch attenuated the  $L$ -type  $Ca^{2+}$  current (Fig. 3A.1), which was estimated as the difference between the negative peak current  $I_{max}$  and the current at the end of the pulse in control ( $I_L$ ) (from  $|1.55|$  nA to  $|1.11|$  nA during

the stretch). The module for  $I_{Ca,L}$  was used because the current value was calculated as a distance (Fig. 3A.1, B.2, C.2) from the starting point (the value of  $I_{Ca,L}$  on the background of nifedipine= $I_L$ , in the positive region) to the point  $I_{max}$ , in the negative region. The time course of the stretch - induced difference of the  $L$ -type  $Ca^{2+}$  current in the control and during the stretch ( $\Delta^S I_{Ca,L}^{tc}$ ) was (+) 0.44 nA ((+)  $0.44 \pm 0.07$  nA,  $n=7$ ). The plus sign indicates that cell stretching at the  $V_{hp} = -45$  mV led to a shift of negative  $I_{Ca,L}$  to more positive values compared to the initial values, resulting in a decrease in the negative area.

The  $I/V$  curves in Fig. 3A.2 show the voltage dependence of  $I_L$  and  $I_{Ca,L}$ , and their modulation by a 6  $\mu\text{m}$  stretch. Before stretching, the  $I_L$  -  $I/V$  curve was  $N$ -shaped and crossed the voltage axis (zero current potential  $V_0$ ) at  $-78$  mV ( $-75 \pm 3$  mV,  $n=7$ ; equivalent to the resting potential of the non-clamped cell). The modest stretch shifted the net currents  $I_L$  to more negative values:  $\Delta^S I_{L(-45)}$  is (-) 0.15 nA ((-)  $0.16 \pm 0.02$  nA,  $n=7$ ) at  $-45$  mV and  $\Delta^S I_{L(-80)}$  is (-) 0.24 nA ((-)  $0.26 \pm 0.03$  nA,  $n=7$ ) at  $-80$  mV. The  $V_0$  also shifted to  $-70$  mV ( $-66 \pm 3$  mV,  $n=7$ ) with the stretch.

During cell stretching, although the changes in the  $I_{L(-45)}$  current occur in the positive range, their values are lower than the control values of  $I_{L(-45)}$ . The minus (-) sign of  $\Delta^S I_{L(-45)}$  emphasizes that cell stretch leads to a change in the curve toward more negative values. Similarly, for  $I_{L(-80)}$ , which is usually in the negative range, cell stretch further increases this negative current  $I_{L(-80)}$ , leading to a negative differential current  $\Delta^S I_{L(-80)}$  that only shows the direction of its change. The  $I/V$  curves recorded before and during the stretch crossed each other close to 0 mV, and at positive potentials, the late current increased with the stretch. The  $I/V$  curve of  $I_{Ca,L}$  decreased during the 6  $\mu\text{m}$  stretch by  $\Delta^S I_{Ca,L} = (+) 0.38$  nA ((+)  $0.32 \pm 0.04$  nA,  $n=7$ ) compared to the control values.

Upon stretching to 8  $\mu\text{m}$ , the holding current  $I_{hc}$  decreased to values close to 0 (label S, Fig. 3B.1), compared to the control holding current (label C, the beginning of the blue traces in this figure). In this case, the stretch-induced difference in the holding current  $\Delta^S I_{hc}$  was (-) 0.41 nA ((-)  $0.42 \pm 0.02$  nA,  $n=7$ ) at  $V_{hp} = -45$  mV. The pulse at 0 mV induced  $I_{Ca,L}$ , and the stretch attenuated  $I_{Ca,L}$  (Fig. 3B.1, negative current wave from blue in control to red during the stretch) from  $|1.55|$  nA in control to  $|0.94|$  nA. During time course registration, the stretch-induced difference of  $L$ -type  $Ca^{2+}$  current in control and during the stretch,  $\Delta^S I_{Ca,L}^{Tc}$  equals (+) 0.61 nA ((+)  $0.60 \pm 0.04$  nA,  $n=7$ ).

Stretching by 8  $\mu\text{m}$  shifted the  $I/V$  relation to more negative currents than a 6  $\mu\text{m}$  stretch (Fig. 3B.2): At  $-45$  mV, the stretch-induced difference in current was  $\Delta^S I_{L(-45)} = (-) 0.29$  nA ((-)  $0.37 \pm 0.06$  nA,  $n=7$ ), while at  $-80$  mV, it was  $\Delta^S I_{L(-80)} = (-) 0.57$  nA ((-)  $0.60 \pm 0.09$  nA,  $n=7$ ), and  $V_0$  was depolarized to  $-56$  mV ( $-54 \pm 3$  mV,  $n=7$ ). The  $I/V$  curve of  $I_{Ca,L}$  during the stretch showed a further decrease in  $I_{Ca,L}$  resulting in an increase in the differential current  $\Delta^S I_{Ca,L}$  to (+) 0.52 nA ((+)  $0.52 \pm 0.02$  nA,  $n=7$ ).

The maximum stretch of 10  $\mu\text{m}$  caused a shift in the holding current  $I_{hc}$  to the negative region with values equal to  $-0.16$  nA (label S, the beginning of the red traces in Fig. 3C.1, compared to label C, the beginning of the blue traces). The stretch-induced difference in the holding current  $\Delta^S I_{hc}$  was (-) 0.61 nA ((-)  $0.74 \pm 0.10$  nA,  $n=7$ )

at  $-45$  mV. This stretch resulted in a further reduction of  $I_{Ca,L}$  (Fig. 3C.1: negative current wave from blue in control to red during the stretch) from  $|1.55|$  nA in control to  $|0.77|$  nA. When registering the time course,  $\Delta^S I_{Ca,L}^{Tc}$  was equal to (+) 0.78 nA ((+)  $0.77 \pm 0.04$  nA,  $n=6$ ).

Stretching the cell by 10  $\mu\text{m}$  caused a larger shift in the  $I/V$  relationship to more negative currents compared to an 8  $\mu\text{m}$  stretch (Fig. 3C.2):  $\Delta^S I_{L(-45)}$  was (-) 0.57 nA ((-)  $0.71 \pm 0.09$  nA,  $n=6$ ) at  $-45$  mV, while  $\Delta^S I_{L(-80)}$  was (-) 1.33 nA ((-)  $1.41 \pm 0.15$  nA,  $n=6$ ) at  $-80$  mV, and depolarized  $V_0$  to  $-35$  mV ( $-39 \pm 3$  mV,  $n=6$ ). During this stretch, the  $I/V$  curve of  $I_{Ca,L}$  showed a larger decrease in  $I_{Ca,L}$ , resulting in an increased differential current  $\Delta^S I_{Ca,L}$  of (+) 0.66 nA ((+)  $0.65 \pm 0.05$  nA,  $n=6$ ).

In  $K^+_{in}/K^+_{out}$  solutions,  $Gd^{3+}$  eliminates stretch-induced reduction in  $I_{Ca,L}$  at all levels of cell stretch, as previously demonstrated [5, 6].

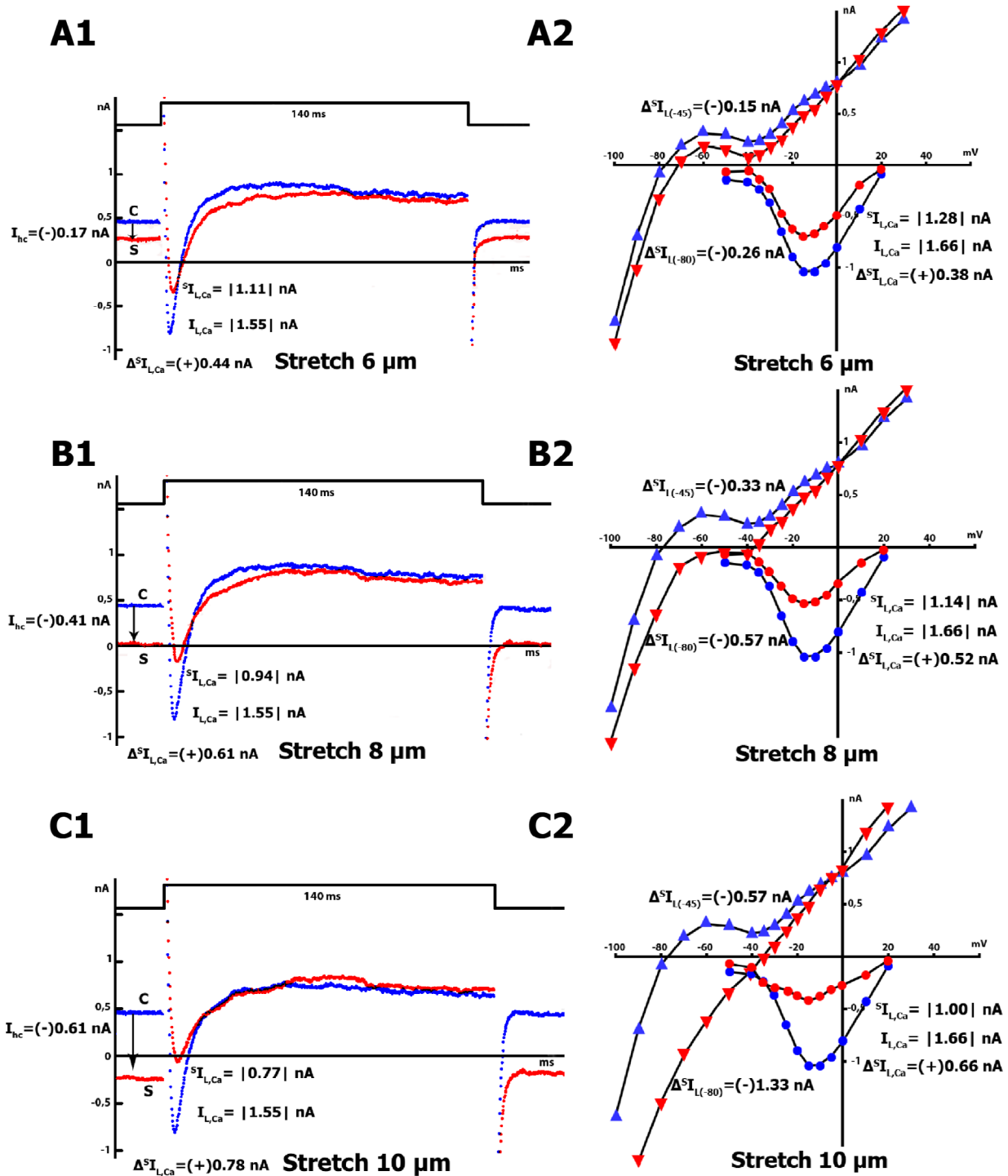
The comparison of the mean values of differential currents  $\Delta^S I_{hc}$ ,  $\Delta^S I_{L(-45)}$ ,  $\Delta^S I_{L(-80)}$ ,  $\Delta^S I_{Ca,L}^{Tc}$  and  $\Delta^S I_{Ca,L}$  during cell stretch at 6, 8, and 10  $\mu\text{m}$  is presented in Fig. 4. It should be noted that  $\Delta^S I_{hc}$ ,  $\Delta^S I_{L(-45)}$ , and  $\Delta^S I_{L(-80)}$  are mechanosensitive and are based on the activation of stretch-activated channels (SAC).

#### Local stretch increased current through nonselective cation channels $I_{ns}$ and, at the same time, reduced $I_{Ca,L}$ in $Cs^+_{in}/Cs^+_{out}$ solutions (time course and voltage dependence).

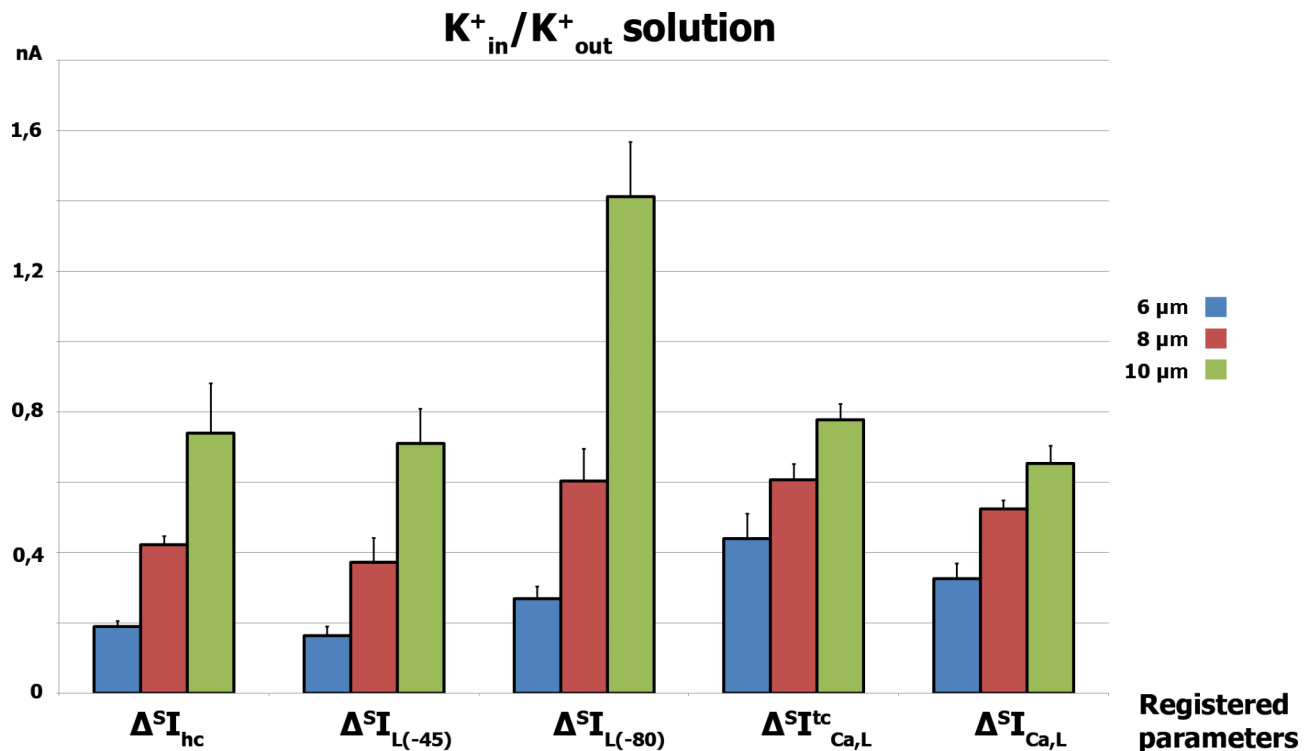
In Fig. 5A.1, the effect of 6  $\mu\text{m}$  stretch on time-dependent membrane currents in  $Cs^+_{in}/Cs^+_{out}$  solutions is presented. At the control stage, the holding current was 0 nA (labeled as C, Fig. 5A.1), while stretch resulted in negative holding current values (labeled as S, Fig. 5A.1). The difference in the holding current induced by stretch was (-) 0.12 nA ( $0.09 \pm 0.01$  nA,  $n=7$ ) at  $-45$  mV. The pulse to 0 mV resulted in an  $L$ -type  $Ca^{2+}$  current of  $-1.49$  nA ( $-1.62 \pm 0.13$  nA,  $n=18$ ), or  $-7.3$  pA/pF ( $-7.1 \pm 0.2$  pA/pF,  $n=18$ ). The stretch of 6  $\mu\text{m}$  reduced the  $L$ -type  $Ca^{2+}$  current,  $I_{Ca,L}$  (as shown by the negative current wave in Fig. 5A.1, from blue to red). During the recording of the time course, the stretch-induced difference of  $L$ -type  $Ca^{2+}$  current in control and during the stretch ( $\Delta^S I_{Ca,L}^{Tc}$ ) was (+) 0.41 nA ((+)  $0.35 \pm 0.05$  nA,  $n=7$ ).

Figure 5 A.2 displays the voltage dependence of  $I_{ns}$ ,  $I_{Ca,L}$  and its modulation by a 6  $\mu\text{m}$  stretch, as shown in the  $I/V$  curves. Before stretching, the  $I/V$  curve of  $I_{ns}$  was linear and intersected the voltage axis (zero current potential  $V_0$ ) at  $-40$  mV ( $-38 \pm 3$  mV,  $n=7$ ). After a modest 6- $\mu\text{m}$  stretch,  $I_{ns}$  shifted to more negative values, and the resulting  $I_{SAC} = I_{ns} - I_{Ca,L}$  (in  $Cs^+_{in}/Cs^+_{out}$  solutions) was (-) 0.10 nA ((-)  $0.09 \pm 0.02$  nA,  $n=7$ ) at  $-45$  mV and (-) 0.14 nA ((-)  $0.12 \pm 0.01$  nA,  $n=7$ ) at  $-80$  mV, while  $V_0$  changed to  $-5$  mV ( $-6 \pm 3$  mV,  $n=7$ ). At potentials close to 0 mV, the  $I/V$  curves recorded before and during the





**Fig. 3** Reduction of  $I_{CaL}$  in  $K^+_{in}/K^+_{out}$  solutions during local stretching of cardiomyocytes by 6, 8, and 10  $\mu$ m.  $V_{hp} = -45$  mV. **A:** (6  $\mu$ m stretch). **A.1** - The time course of the membrane current. The holding current at  $V_{hp}$  in control (beginning of the blue traces - label C) and during stretching (beginning of the red traces - label S). A pulse from  $-45$  to  $0$  mV induces  $I_{CaL}$ , which decreases during stretching (indicated by a negative blue current wave compared to a negative red wave). **A.2** - I/V curve of  $I_L$  before (blue triangles) and during (red triangles) stretching, as well as  $I_{CaL}$  before (blue circles) and during (red circles) stretching. **B:** (8  $\mu$ m stretch). **B.1** - The time course of the membrane current before and during stretching, which results in a greater reduction of  $I_{CaL}$  compared to A.1. Notations as in A.1. **B.2** - I/V curves of  $I_L$  and  $I_{CaL}$  before and during stretching. Notations as in A.2. **C:** (10  $\mu$ m stretch). **C.1** - The time course of the membrane current in control and during stretching.  $I_{CaL}$  decreases with increasing stretching. Notations as in A.1. **C.2** - I/V curves of  $I_L$  and  $I_{CaL}$  before and during stretching. Notations as in A.2.



**Fig. 4** Comparison of the mean values of the differential currents  $\Delta S I_{hc}$ ,  $\Delta S I_{L(-45)}$ ,  $\Delta S I_{L(-80)}$ ,  $\Delta S I_{Ca,L}^{tc}$  and  $\Delta S I_{Ca,L}$  during cell stretching at 6, 8, and 10  $\mu\text{m}$  in  $K^+_{in}/K^+_{out}$  solutions. Error bars represent  $\pm$ SD for  $n$  experiments ( $n = 7$ )

stretch intersected, while at positive potentials,  $I_{ns}$  exhibited an increase due to the stretch. Furthermore, the  $I/V$  curve of  $^S I_{Ca,L}$  during the stretch decreased from  $-1.27$  nA in the control to  $-1.00$  nA, resulting in a  $\Delta S I_{Ca,L}$  of  $(+) 0.27$  nA  $(+ 0.34 \pm 0.06$  nA,  $n = 7$ ) when compared to the control values.

When subjected to an 8  $\mu\text{m}$  stretch, the difference in the holding current at  $-45$  mV changed to values close to  $(-) 0.17$  nA  $(- 0.16 \pm 0.301$  nA,  $n = 7$ ; labeled S, Fig. 5B.1, compared to label C in the figure). The pulse from  $-45$  to 0 mV induced  $I_{Ca,L}$ , but the 8  $\mu\text{m}$  stretch attenuated  $^S I_{Ca,L}$  (as seen in Fig. 5B.1, where the negative current wave shifts from blue to red during the stretch), from  $-1.49$  nA in the control to  $-0.86$  nA. When the time course was registered,  $\Delta S I_{Ca,L}^{tc}$  was calculated to be  $(+) 0.63$  nA  $(+ 0.64 \pm 0.06$  nA,  $n = 7$ ).

The 8  $\mu\text{m}$  stretch caused a shift in the  $I/V$  relation to more negative currents compared to the 6  $\mu\text{m}$  stretch (as seen in Fig. 5B.2):  $I_{SAC(-45)}$  was  $(-) 0.16$  nA  $(- 0.16 \pm 0.02$  nA,  $n = 7$ ) at  $-45$  mV, and  $I_{SAC(-80)}$  was  $(-) 0.25$  nA  $(- 0.18 \pm 0.04$  nA,  $n = 7$ ) at  $-80$  mV. During this stretch, the  $I/V$  curve of  $I_{Ca,L}$  further decreased  $^S I_{Ca,L}$  from  $-1.27$  to  $-0.54$  nA, resulting in an increase in differential current  $\Delta S I_{Ca,L}$  to  $(+) 0.73$  nA  $(+ 0.62 \pm 0.09$  nA,  $n = 7$ ) compared to control values.

The longest 10  $\mu\text{m}$  stretch caused a shift of the holding current to the negative region (label S, Fig. 5C.1,

compared to label C). The stretch-induced difference in the holding current was  $(-) 0.35$  nA  $(- 0.34 \pm 0.02$  nA,  $n = 7$ ) at  $-45$  mV. Furthermore, this stretch reduced  $^S I_{Ca,L}$  even more (Fig. 5C.1), from  $-1.49$  nA in the control to  $-0.74$  nA. In the case of time course registration,  $\Delta S I_{Ca,L}^{tc}$  equals  $(+) 0.75$  nA  $(+ 0.75 \pm 0.05$  nA,  $n = 7$ ).

Stretching by 10  $\mu\text{m}$  shifted the  $I/V$  relation to more negative currents than an 8  $\mu\text{m}$  stretch (Fig. 5C.2). Specifically,  $I_{SAC(-45)}$  was  $(-) 0.32$  nA  $(- 0.34 \pm 0.05$  nA,  $n = 7$ ) and  $I_{SAC(-80)}$  was  $(-) 0.53$  nA  $(- 0.48 \pm 0.10$  nA,  $n = 7$ ). The 10- $\mu\text{m}$  stretch further reduced  $^S I_{Ca,L}$  to  $-0.38$  nA (Fig. 5C.2, red circles), resulting in an increase in differential current  $\Delta S I_{Ca,L}$  to  $(+) 0.89$  nA  $(+ 0.79 \pm 0.09$  nA,  $n = 7$ ).

In  $Cs^+_{in}/Cs^+_{out}$  solutions,  $Gd^{3+}$  eliminates the reduction of stretch-induced  $I_{Ca,L}$  as well as  $\Delta S I_{L(-45)}$ ,  $\Delta S I_{L(-80)}$ , as previously demonstrated in our studies [5, 6] (not shown in Fig. 5).

Figure 6 compares the mean values of  $I_{SAC(hc)}$ ,  $I_{SAC(-45)}$ ,  $I_{SAC(-80)}$ ,  $^S I_{Ca,L}$ , and  $\Delta S I_{Ca,L}$  during cell stretching at 6, 8, and 10  $\mu\text{m}$  in  $Cs^+_{in}/Cs^+_{out}$  solutions.  $I_{SAC(hc)}$ ,  $I_{SAC(-45)}$ , and  $I_{SAC(-80)}$  are also mechanosensitive currents based on the work of SAC. Additionally,  $I_{Ca,L}$  is likely to be conducted through  $Ca_v1.2$  channels and is also mechanosensitive in ventricular rat cardiomyocytes.

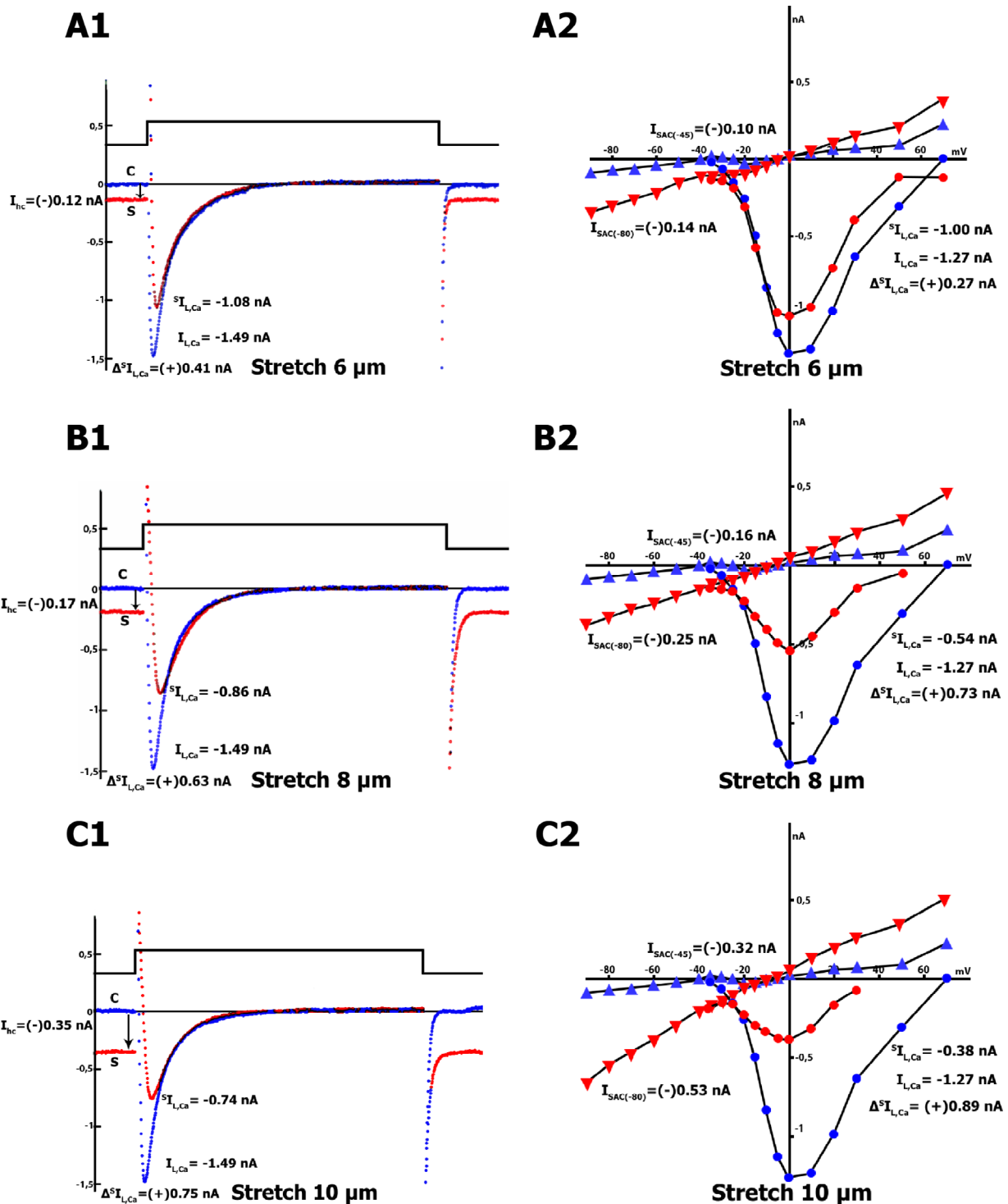


**Fig. 5** Reduction of  $I_{Ca,L}$  in  $CS_{in}^+/CS_{out}^+$  solutions with  $K^+$  currents suppressed during local stretching of cardiomyocytes by 6, 8, and 10  $\mu\text{m}$ .  $V_{hp} = -45 \text{ mV}$ . **A:** (6  $\mu\text{m}$  stretch). **A.1** – The time course of the membrane current. The holding current at  $V_{hp}$  in control (beginning of the blue traces - label C) and during stretching (beginning of the red traces – label S). A pulse from  $-45$  to  $0 \text{ mV}$  induces  $I_{Ca,L}$ , which decreases during stretching (indicated by a negative blue current wave compared to a negative red wave). **A.2** –  $I/V$  curve of  $I_{ns}$  before (blue triangles) and during (red triangles) stretching, as well as  $I_{Ca,L}$  before (blue circles) and during (red circles) stretching. **B:** (8  $\mu\text{m}$  stretch). **B.1** – The time course of the membrane current before and during stretching, which results in a greater reduction of  $I_{Ca,L}$  compared to **A.1**. Notations as in **A.1**. **B.2** –  $I/V$  curves of  $I_{ns}$  and  $I_{Ca,L}$  before and during stretching. Notations as in **A.2**. **C:** (10  $\mu\text{m}$  stretch). **C.1** – The time course of the membrane current in control and during stretching.  $I_{Ca,L}$  decreases with increasing stretching. Notations as in **A.1**. **C.2** –  $I/V$  curves of  $I_{ns}$  and  $I_{Ca,L}$  before and during stretching. Notations as in **A.2**

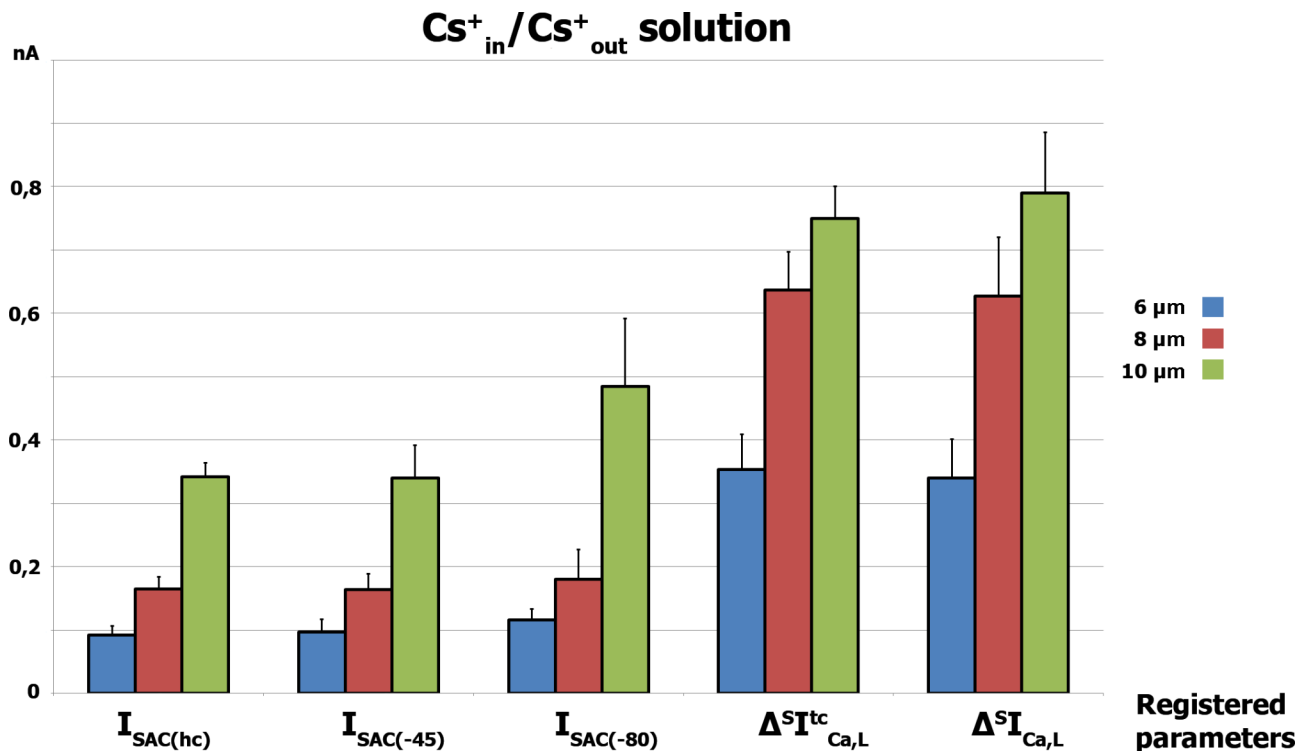


**Fig. 6** Comparison of the mean values of the differential currents  $I_{SAC(hc)}$ ,  $I_{SAC(-45)}$ ,  $I_{SAC(-80)}$ ,  $\Delta^{ST}I_{Ca,L}$  and  $\Delta^S I_{Ca,L}$  during cell stretching at 6, 8, and 10  $\mu\text{M}$  in  $\text{Cs}^+_{in}/\text{Cs}^+_{out}$  solutions. The  $\pm$  SD is shown for  $n$  experiments ( $n=7$ )

### $\text{Gd}^{3+}$ eliminates the $L$ -type $\text{Ca}^{2+}$ current via $\text{Ca}_v1.2$ channels in $\text{K}^+_{in}/\text{K}^+_{out}$ , $\text{Cs}^+_{in}/\text{K}^+_{out}$ , $\text{K}^+_{in}/\text{Cs}^+_{out}$ and $\text{Cs}^+_{in}/\text{Cs}^+_{out}$ solutions

Figure 7. A, B, C, and D illustrate that  $I_{Ca,L}$  values remained constant ( $1.48 \pm 0.06$  nA,  $n=24$ ) under all experimental conditions tested, including  $\text{K}^+_{in}/\text{K}^+_{out}$ ,  $\text{Cs}^+_{in}/\text{K}^+_{out}$ ,  $\text{K}^+_{in}/\text{Cs}^+_{out}$ , and  $\text{Cs}^+_{in}/\text{Cs}^+_{out}$  solutions. Furthermore, during the transition of cell perfusion from  $\text{K}^+_{in}/\text{K}^+_{out}$  to  $\text{K}^+_{in}/\text{Cs}^+_{out}$  solutions (Fig. 7C),  $I_{Ca,L}$  values did not change ( $n=6$ ). The  $I_{Ca,L}$  values were determined by calculating the maximum calcium peak current at a given potential at the point on the late current curve that corresponds to that potential. For  $\text{Cs}^+_{in}/\text{Cs}^+_{out}$  solutions, two variants of  $I_{Ca,L}$  values were presented (Fig. 7B): (1) up to zero and (2) up to a characteristic point on the late current curve. Typically, only the value (1) is used for calculations in the literature.

It has been shown that, on the background of cell stretch,  $\text{Gd}^{3+}$  at a concentration of 5  $\mu\text{M}$  blocks  $I_{SAC}$  [6]. The addition of  $\text{Gd}^{3+}$  abolished the dependence of  $I_{SAC}$  on all local stretch values. Our experiments revealed that  $\text{Gd}^{3+}$  also had a minor inhibitory effect on the  $I_L$  current at  $-45$  and  $-80$  mV, suggesting that  $I_{SAC}$  may have contributed to the net currents of the non-stretched cells. This is depicted in Fig. 7, where the blue triangles indicate the control and the red triangles indicate the application

of the blocker ( $n=6$ ). Additionally,  $\text{Gd}^{3+}$  did not affect the background current,  $I_{Kl}$  (Fig. 7A).

To investigate potential changes in  $L$ -type  $\text{Ca}^{2+}$  current through  $\text{Ca}_v1.2$  channels, we applied  $\text{Gd}^{3+}$ , which is known to be a nonspecific blocker of the mechanically gated channel's current  $I_{SAC}$ . Our results indicated that the addition of 5  $\mu\text{M}$  of  $\text{Gd}^{3+}$  eliminated  $L$ -type  $\text{Ca}^{2+}$  current in  $\text{K}^+_{in}/\text{K}^+_{out}$  ( $n=6$ ),  $\text{Cs}^+_{in}/\text{K}^+_{out}$  ( $n=6$ ),  $\text{K}^+_{in}/\text{Cs}^+_{out}$  ( $n=6$ ), and  $\text{Cs}^+_{in}/\text{Cs}^+_{out}$  ( $n=6$ ) solutions (blue circles in the control compared to red circles after application of the blocker).

## Discussion

### Channel transcripts and their mechanosensitivity

In ventricular cardiomyocytes, mechanosensitive channels are believed to play a role in the regulation of the contractile properties of the heart [5]. In our experiments, we found significant amounts of transcripts for the mechanosensitive channels TRPM7, TRPC1, and TRPM4 (Table 1).

TRPM7 is a nonselective cation channel that is permeable to both  $\text{Ca}^{2+}$  and  $\text{Mg}^{2+}$  [102]. It has been shown to contribute to the stretch-induced current in ventricular cardiomyocytes by mediating a  $\text{Ca}^{2+}$  influx in response to mechanical stretch [103, 104]. This influx of  $\text{Ca}^{2+}$  is believed to activate downstream signaling pathways that regulate contractility [103]. TRPC1 was shown to

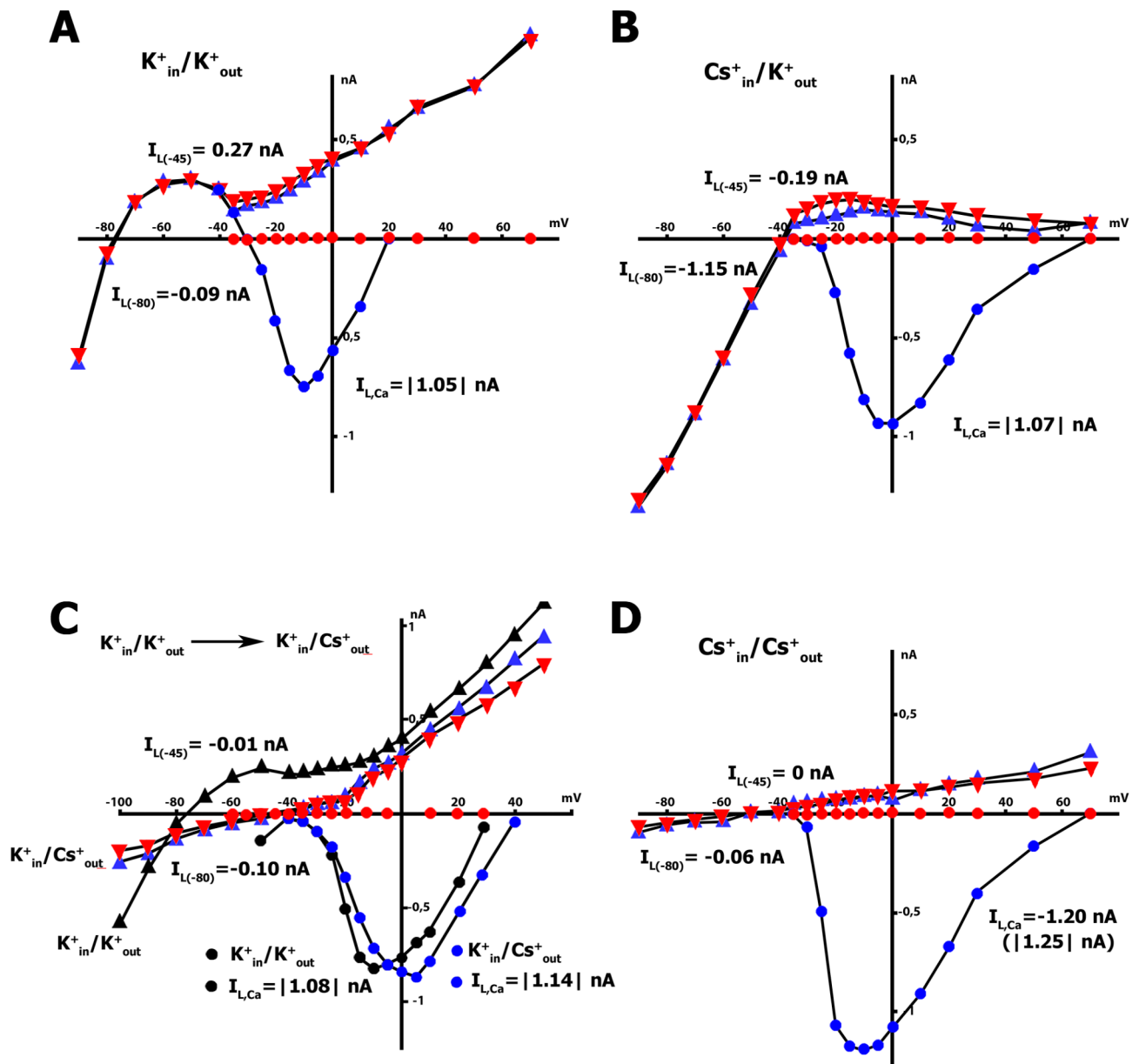


**Fig. 7** Effect of 5  $\mu$ M  $Gd^{3+}$  on  $I_L$  and  $I_{CaL}$  in  $K^+_{in}/K^+_{out}$  (A),  $Cs^+_{in}/K^+_{out}$  (B),  $K^+_{in}/Cs^+_{out}$  (C), and  $Cs^+_{in}/Cs^+_{out}$  (D) solutions. Control curves in blue:  $I_L$  – triangles and  $I_{CaL}$  – circles. Curves in the presence of  $Gd^{3+}$  in red:  $I_L$  – triangles and  $I_{CaL}$  – circles. Note: C: Switching cell perfusion from  $K^+_{in}/K^+_{out}$  solution ( $I_L$  – black triangles and  $I_{CaL}$  – black circles) to  $K^+_{in}/Cs^+_{out}$  solution ( $I_L$  – blue triangles and  $I_{CaL}$  – blue circles), followed by the application of  $Gd^{3+}$  ( $I_L$  – red triangles and  $I_{CaL}$  – red circles). While  $Gd^{3+}$  exerts only a minor effect on  $I_L$  it eliminates  $I_{CaL}$  in all solutions tested

contribute to the stretch-induced current in ventricular cardiomyocytes by mediating a non-selective cation influx in response to mechanical stretch, which influx is believed to depolarize the cell membrane and contribute to the regulation of contractility [104]. TRPM4 is a  $Ca^{2+}$ -activated non-selective cation channel that has been shown to contribute to the stretch-induced current in ventricular cardiomyocytes [45]. It is believed to be activated by  $Ca^{2+}$  influx through other channels such as TRPC1 and TRPM7 [37, 42, 105]. TRPM4 activation is

believed to contribute to contractility regulation by modulating the duration of AP [106].

Studies on mechanosensitivity in murine ventricular myocytes have shown a link between stretch-activated TRPC6 channels as well as stretch-deactivated GK1 and especially Kir2.3 channels [22]. GK1 channels are formed by Kir2.1, Kir2.2, and Kir2.3 proteins [107, 108]. In our experiments, we found multiple transcripts of Kir2.1 and Kir2.2 in isolated ventricular myocytes from rats, while Kir2.3 was absent. Therefore, in  $K^+_{in}/K^+_{out}$  solutions, the mechanosensitivity of ventricular myocytes is probably



determined by the stretch-activated TRPM7, TRPC1, and TRPM4 channels and the stretch-deactivated GK1 (Kir2.1 and Kir2.2) channels. Our findings are consistent with other studies [109], which have shown that ventricular  $I_{K1}$  is based primarily on the heteromeric assembly of the Kir2.1 and Kir2.2 channels, while the Kir2.3 channels are more relevant in the atrium.

### The local stretch of cells modulates $I_{Ca,L}$ probably through $Ca_v1.2$ channels

One of the main questions of the study was to determine the cause of changes in  $I_{Ca,L}$ . Our observations showed a decrease in  $^S I_{Ca,L}$  with discrete cell stretching, while there was a corresponding increase in  $\Delta^{S_{Tc}} I_{Ca,L}$  and  $\Delta^S I_{Ca,L}$  during cell stretching at 6, 8, and 10  $\mu\text{m}$ .

In general, membrane channels (including voltage-gated) are expected to respond to mechanical stimuli because mechanical energy can affect the energy barriers between different conformational states of a channel protein [110]. For example, longitudinal stretching has been shown to modify the gating mechanism of;  $Na_v$  channels [111], such as  $Na_v1.5$  [81, 82] and  $Na_v1.6$  [83],  $Ca_v$  channels such as  $Ca_v1.2$  [84],  $Ca_v1.3$  [85], and  $Ca_v2.2$  channels [86], as well as  $K_v$  channels such as  $K_v1.2$  [67],  $K_v1.5$ , and  $K_v3.2$  [87, 112]. In addition, mechanical energy can affect the conformation of proteins associated with cytoskeletal elements [113, 114], such as F-actin [114] and integrins [115]. This can also activate stretch-sensitive kinases (Src, MAP) or phosphatases, which can, in turn, modulate the channel protein by phosphorylation and dephosphorylation [109]. Finally, mechanical stretch can also impact the production rate of reactive oxygen species, or NO, which can modify channel gating through oxidative or nitrosative mechanisms [116], which in turn can play a role in stretch-induced effects on  $Ca^{2+}$  release from the sarcoplasmic reticulum (SR) [116, 117].

The *L-type*  $Ca^{2+}$  current is responsible for generating the negative current wave observed at the start of the depolarizing clamp step (Fig. 3A.1, B.1, and C.1), as well as the long-lasting plateau of the AP. Interestingly, the local mechanical stretch has been shown to decrease  $I_{Ca,L}$  with the reduction being observed across the entire range of clamp potentials. In particular, the voltage dependence of  $I_{Ca,L}$  appears to remain unchanged under these conditions (see Fig. 3A.2, B.3, and C.4).

In ventricular myocytes, some nonselective channels are known to be activated by an increase in cytosolic calcium concentration ( $[Ca^{2+}]_C$ ) [118]. To investigate whether stretch-induced changes in  $[Ca^{2+}]_C$  might play a role in these effects, Gannier et al. (1996) conducted experiments in which they prevented possible stretch-induced increments in  $[Ca^{2+}]_C$  [119]. Interestingly, they have found that chelation of the  $[Ca^{2+}]_C$  does not have a significant effect on  $I_{SAC}$ . However, we observed

significant effects of BAPTA on the stretching effects on  $I_{Ca,L}$ . Specifically, while  $I_{SAC}$  in  $Cs^+_{in}/Cs^+_{out}$  solutions was found to be insensitive to chelation of  $[Ca^{2+}]_C$ , the stretch-induced reduction of  $I_{Ca,L}$  disappeared after dialyzing the cell with 5 mM BAPTA in the patch pipette [6].

Since stretch has been shown to increase  $[Ca^{2+}]_C$  and BAPTA can chelate cytosolic  $Ca^{2+}$ , it is likely that the stretch-induced reduction of  $^S I_{Ca,L}$  results from the stretch-induced increase in  $[Ca^{2+}]_C$  followed by  $Ca^{2+}$ -mediated inactivation of the  $Ca^{2+}$  channel ( $Ca^{2+}$ -calmodulin interaction with the  $Ca^{2+}$  channel  $\alpha$  subunit) [12]. We propose that the primary effect of stretch is to increase  $[Ca^{2+}]_C$  via an increase in  $Ca^{2+}$  influx through SACs or via  $Ca^{2+}$  release from the SR in the vicinity of the L-type  $Ca^{2+}$  channel. Previous research has suggested that  $I_{Ca,L}$  can be reduced by an increase in  $[Ca^{2+}]_C$  and by stimulation of  $I_p$  (current due to electrogenic sodium pumping) by an increase in  $[Na^+]_C$ . The concept of indirect activation by stretch should also be applied to the current generated by  $Na^+/Ca^{2+}$ -exchange if  $[Na^+]$  is elevated by  $Na^+$  influx due to  $I_{SAC}$  [120] and to  $K^+$  channels activated by  $Ca^{2+}$  or  $Na^+$  ions [121]. Alternatively, the stretch may increase  $[Ca^{2+}]_C$  by  $Ca^{2+}$  release from the SR [117].

Cytoskeletal F-actin fibers were found to be involved specifically in  $I_{SAC}$  activation and regulation of the  $Ca_v1.2$  channel gating mechanism. In the context of cell stretch, which has been shown to increase  $I_{SAC}$  and decrease  $I_{Ca,L}$ , treatment with cytochalasin D, a toxin known to depolymerize F-actin, blocks the effects of stretch on late currents and leads to further reduction of  $I_{Ca,L}$  [8], which also corroborates the effect of cell stretch, probably on the  $Ca_v1.2$  channel.

We make such an assumption based on the analysis of the transcript quantities for  $Ca^{2+}$  ion channel genes. As we have demonstrated, the transcript counts for the  $Ca_v1.2$  channel gene are exceptionally high, measuring  $1336.66 \pm 71.8$ . In contrast, for  $Ca_v1.3$ , this count is quite low at  $17.33 \pm 2.03$ , and for  $Ca_v1.1$ , it is minimal at  $0.33 \pm 0.33$ . We did not detect other channels involved in the whole *L-type*  $Ca^{2+}$  current. Based on these numerical values, we can infer the primary role of the  $Ca_v1.2$  channel in the formation of the *L-type*  $Ca^{2+}$  current that we observed.

### Voltage-gated current modulation or mechanosensitivity of the ( $Ca_v1.2$ ) channel

It is now well established that  $Gd^{3+}$  blocks a range of ion channels, including SACs (mechanically gated nonselective cation channels,  $MGC_{ns}$ , and mechanically gated potassium channels,  $MGC_K$ ), which was previously assumed in the study by Yang et al. (1989) [122]. In addition,  $Gd^{3+}$  has been found to block several other ion channels, such as  $BK_{Ca}$  channels cloned from chick

ventricular myocytes [123] and *delayed rectifier current* ( $I_K$ ) in guinea pig single ventricular myocytes, including both  $I_{KR}$  (rapidly activated) and  $I_{KS}$  (slowly activated), while the background current  $I_{K1}$ , was not affected by  $Gd^{3+}$  [124]. Moreover,  $Gd^{3+}$  was a potent  $I_{Na}$  blocker near the threshold potential for  $Na^+$  channels in rabbit ventricular myocytes [122]. It has been demonstrated that  $Gd^{3+}$  is also a potent blocker of L-type  $Ca^{2+}$  channels in isolated guinea pig ventricular myocytes [125].

In our experiments, treatment with the nonspecific inhibitor of  $I_{SAC}$ ,  $Gd^{3+}$ , on the background of cell stretching eliminated both  $I_{SAC}$  and  $I_{Ca,L}$  at all stretching magnitudes and voltage steps relative to the  $V_{hp}$ . This response to  $Gd^{3+}$  was maintained in  $Cs^+_{in}/Cs^+_{out}$  solutions, indicating that voltage-gated channels, apparently  $Ca_v1.2$  in adult rat ventricular myocytes, have additional mechanosensitive properties.

## Conclusion

Our analysis revealed the presence of transcripts for the TRPM7, TRPC1, and TRPM4 channels that are known to exhibit mechanosensitivity. Furthermore, we detected mechanosensitive transcripts of the Kir6.2 and Kir6.1 channels, as well as transcripts of GK1 channels formed by the Kir2.1 and Kir2.2 proteins. Although the detection of the TREK-1/ $K_{2p2.1}$  transcript was limited, indirect data from other studies supports its presence [77]. The highest number of RNA reads among all  $Ca_v$  channels was detected for  $Ca_v1.2$  channels, which themselves exhibit mechanosensitivity.

Cell stretching at various magnitudes discretely increased  $I_{SAC}$  and decreased  $I_{Ca,L}$  probably through  $Ca_v1.2$  channels in  $K^+_{in}/K^+_{out}$ ,  $Cs^+_{in}/K^+_{out}$ ,  $K^+_{in}/Cs^+_{out}$ , and  $Cs^+_{in}/Cs^+_{out}$  solutions. However, treatment with the nonspecific blocker of  $I_{SAC}$ ,  $Gd^{3+}$ , on the background of cell stretching eliminated both  $I_{SAC}$  and  $I_{Ca,L}$  at all stretching magnitudes and voltage steps relative to  $V_{hp}$ . The study suggests that voltage-gated  $Ca_v1.2$  channels in adult rat ventricular myocytes have additional mechanosensitive properties, as evidenced by the maintained response to  $Gd^{3+}$  in the  $Cs^+_{in}/Cs^+_{out}$  solution.

## Supplementary Information

The online version contains supplementary material available at <https://doi.org/10.1186/s13062-023-00427-0>.

Supplementary Material 1

## Acknowledgements

Not applicable.

## Authors' contributions

Substantial contributions to the conception or design of the work: A.G.K., O.V.K., and V.E.K. Substantial contributions to the acquisition, analysis, or interpretation of data for the work: A.G.K., V.E.K., O.V.K., V.M.M., A.B., A.S.R., A.D.Z., V.I.Z., E.A.N., S.A.S., P.V.S. and M.I.M. Drafting the work or revising it critically

for important intellectual content: A.G.K. Final approval of the version to be published: A.G.K., O.V.K., V.E.K., V.M.M., A.B., A.S.R., A.D.Z., V.I.Z., E.A.N., S.A.S., P.V.S., and M.I.M.

## Funding

The authors declare that no funds, grants, or other support were received during the preparation of this manuscript.

## Data Availability

The datasets generated during and/or analyzed during the current study are available in the following repository [[https://disk.yandex.ru/d/40Xg\\_q8soUg7AA](https://disk.yandex.ru/d/40Xg_q8soUg7AA)].

## Declarations

### Competing interests

The authors declare no competing interests.

### Ethics approval

All experiments in this study were approved by the Ethics Committee of the Russian National Research Medical University according to the guidelines issued by the Guide for Care and Use of Laboratory Animals (8th edition, 2011) published by the US National Institutes of Health and ARRIVE guidelines.

### Consent for publication

Not applicable.

Received: 19 June 2023 / Accepted: 13 October 2023

Published online: 30 October 2023

## References

1. Kaufmann R, Theophile U. Autonomously promoted extension effect in Purkinje fibers, papillary muscles and trabeculae carneae of rhesus monkeys. *Pflugers Arch Gesamte Physiol Menschen Tiere*. 1967;297:174–89.
2. Nazir SA, Lab MJ. Mechanoelectric feedback and atrial arrhythmias. *Cardiovasc Res*. 1996;32:52–61.
3. Dobrev D, Ravens U. Remodeling of cardiomyocyte ion channels in human atrial fibrillation. *Basic Res Cardiol*. 2003;98:137–48. <https://doi.org/10.1007/s00395-003-0409-8>.
4. Craelius W, Chen V, el-Sherif N. Stretch activated ion channels in ventricular myocytes. *Biosci Rep*. 1988;8:407–14. <https://doi.org/10.1007/BF01121637>.
5. Kamkin A, Kiseleva I, Isenberg G. Stretch-activated currents in ventricular myocytes: amplitude and arrhythmogenic effects increase with hypertrophy. *Cardiovascular Res*. 2000;48:409–20. [https://doi.org/10.1016/S0008-6363\(00\)00208-X](https://doi.org/10.1016/S0008-6363(00)00208-X).
6. Kamkin A, Kiseleva I, Isenberg G. Ion selectivity of stretch-activated cation currents in mouse ventricular myocytes. *Pflugers Arch - Eur J Physiol*. 2003;446:220–31. <https://doi.org/10.1007/s00424-003-1018-y>.
7. Zeng T, Bett GCL, Sachs F. Stretch-activated whole cell currents in adult rat cardiac myocytes. *Am J Physiol Heart Circ Physiol*. 2000;278:548–57. <https://doi.org/10.1152/ajpheart.2000.278.2.H548>.
8. Kamkin A, Kiseleva I, Wagner K-D, Bohm J, Theres H, Günther J, et al. Characterization of stretch-activated ion currents in isolated atrial myocytes from human hearts. *Pflugers Arch - Eur J Physiol*. 2003;446:339–46. <https://doi.org/10.1007/s00424-002-0948-0>.
9. Bustamante JO, Ruknudin A, Sachs F. Stretch-activated channels in heart cells: relevance to cardiac hypertrophy. *J Cardiovasc Pharmacol*. 1991;17(Suppl 2):110–3. <https://doi.org/10.1097/00005344-199117002-00024>.
10. Kim D. Novel cation-selective mechanosensitive ion channel in the atrial cell membrane. *Circ Res*. 1993;72:225–31. <https://doi.org/10.1161/01.res.72.1.225>.
11. Ruknudin A, Sachs F, Bustamante JO. Stretch-activated ion channels in tissue-cultured chick heart. *Am J Physiol*. 1993;264. <https://doi.org/10.1152/ajpheart.1993.264.3.H960>. :H960-972.
12. Sigurdson W, Ruknudin A, Sachs F. Calcium imaging of mechanically induced fluxes in tissue-cultured chick heart: role of stretch-activated ion channels. *Am J Physiol*. 1992;262:H1110–1115. <https://doi.org/10.1152/ajpheart.1992.262.4.H1110>.

13. None FGEW, Jy G. LG. A possible mechanism for large stretch-induced increase in  $[Ca^{2+}]_i$  in isolated guinea-pig ventricular myocytes. *Cardiovascular research* [Internet]. 1996 [cited 2023 Sep 29];32. <https://pubmed.ncbi.nlm.nih.gov/8776413/>.
14. Youm JB, Han J, Kim N, Zhang Y-H, Kim E, Leem CH, et al. Role of Stretch-activated channels in the heart: action potential and  $Ca^{2+}$  transients. In: Kamkin A, Kiseleva I, editors. *Mechanosensitivity in cells and tissues*. Moscow: Academia; 2005. <http://www.ncbi.nlm.nih.gov/books/NBK7490/>.
15. Youm JB, Han J, Kim N, Zhang Y-H, Kim E, Joo H, et al. Role of stretch-activated channels on the stretch-induced changes of rat atrial myocytes. *Prog Biophys Mol Biol*. 2006;90:186–206. <https://doi.org/10.1016/j.pbiomolbio.2005.06.003>.
16. Belus A, White E. Streptomycin and intracellular calcium modulate the response of single guinea-pig ventricular myocytes to axial stretch. *J Physiol*. 2003;546:501–9. <https://doi.org/10.1113/jphysiol.2002.027573>.
17. Hongo K, White E, Le Guennec JY, Orchard CH. Changes in  $[Ca^{2+}]_i$ ,  $[Na^+]_i$ , and  $Ca^{2+}$  current in isolated rat ventricular myocytes following an increase in cell length. *J Physiol*. 1996;491(Pt 3):609–19.
18. Sasaki N, Mitsuiye T, Noma A. Effects of mechanical stretch on membrane currents of single ventricular myocytes of guinea-pig heart. *Jpn J Physiol*. 1992;42:957–70. <https://doi.org/10.2170/jjphysiol.42.957>.
19. White E, Boyett MR, Orchard CH. The effects of mechanical loading and changes of length on single guinea-pig ventricular myocytes. *J Physiol*. 1995;482:93–107. <https://doi.org/10.1113/jphysiol.1995.sp020502>.
20. Calaghan SC, Belus A, White E. Do stretch-induced changes in intracellular calcium modify the electrical activity of cardiac muscle? *Progress in Biophysics and Molecular Biology*. 2003;82:81–95. [https://doi.org/10.1016/S0079-6107\(03\)00007-5](https://doi.org/10.1016/S0079-6107(03)00007-5).
21. Isenberg G, Klöckner U. Calcium currents of isolated bovine ventricular myocytes are fast and of large amplitude. *Pflügers Arch*. 1982;395:30–41. <https://doi.org/10.1007/BF00584965>.
22. Dyachenko V, Husse B, Rueckschloss U, Isenberg G. Mechanical deformation of ventricular myocytes modulates both TRPC6 and Kir2.3 channels. *Cell Calcium*. 2009;45:38–54. <https://doi.org/10.1016/j.ceca.2008.06.003>.
23. Babraham Bioinformatics - FastQC A Quality Control tool for High Throughput Sequence Data. <https://www.bioinformatics.babraham.ac.uk/projects/fastqc/>.
24. Bolger AM, Lohse M, Usadel B. Trimmomatic: a flexible trimmer for Illumina sequence data. *Bioinformatics*. 2014;30:2114–20. <https://doi.org/10.1093/bioinformatics/btu170>.
25. Chen S, Zhou Y, Chen Y, Gu J. Fastp: an ultra-fast all-in-one FASTQ preprocessor. *Bioinformatics*. 2018;34:i884–90. <https://doi.org/10.1093/bioinformatics/bty560>.
26. Kim D, Langmead B, Salzberg SL. HISAT: a fast spliced aligner with low memory requirements. *Nat Methods*. 2015;12:357–60. <https://doi.org/10.1038/nmeth.3317>.
27. Li H, Handsaker B, Wysoker A, Fennell T, Ruan J, Homer N, et al. The sequence Alignment/Map format and SAMtools. *Bioinformatics*. 2009;25:2078–9. <https://doi.org/10.1093/bioinformatics/btp352>.
28. Anders S, Pyl PT, Huber W. HTSeq—a Python framework to work with high-throughput sequencing data. *Bioinformatics*. 2015;31:166–9. <https://doi.org/10.1093/bioinformatics/bty638>.
29. Verheijck EE, van Ginneken AC, Wilders R, Bouman LN. Contribution of L-type  $Ca^{2+}$  current to electrical activity in sinoatrial nodal myocytes of rabbits. *Am J Physiol*. 1999;276:1064–77. <https://doi.org/10.1152/ajpheart.1999.276.3.H1064>.
30. Galli GLJ, Taylor EW, Shiels HA. Calcium flux in turtle ventricular myocytes. *Am J Physiol Regul Integr Comp Physiol*. 2006;291:1781–9. <https://doi.org/10.1152/ajpregu.00421.2006>.
31. Sagawa H, Hoshino S, Yoshioka K, Ding W-G, Omatsu-Kanbe M, Nakagawa M, et al. Postnatal developmental changes in the sensitivity of L-type  $Ca^{2+}$  channel to inhibition by verapamil in a mouse heart model. *Pediatr Res*. 2018;83:1207–17. <https://doi.org/10.1038/pr.2018.46>.
32. Dyachenko V, Rueckschloss U, Isenberg G. Modulation of cardiac mechano-sensitive ion channels involves superoxide, nitric oxide and peroxynitrite. *Cell Calcium*. 2009;45:55–64. <https://doi.org/10.1016/j.ceca.2008.06.002>.
33. Boycott HE, Barbier CSM, Eichel CA, Costa KD, Martins RP, Louault F, et al. Shear stress triggers insertion of voltage-gated potassium channels from intracellular compartments in atrial myocytes. *Proc Natl Acad Sci U S A*. 2013;110:3955–64. <https://doi.org/10.1073/pnas.1309896110>.
34. Kamkin A, Kiseleva I, Wagner K-D, Scholz H. Mechano-Electrical Feedback in the heart: evidence from intracellular microelectrode recordings on multicellular preparations and single cells from healthy and diseased tissue. In: Kamkin A, Kiseleva I, editors. *Mechanosensitivity in cells and tissues*. Moscow: Academia; 2005. <http://www.ncbi.nlm.nih.gov/books/NBK7502/>.
35. Lozinsky I, Kamkin A. Mechanosensitive alterations of action potentials and membrane currents in healthy and diseased cardiomyocytes: Cardiac tissue and isolated cell. In: Kamkin A, Kiseleva I, editors. *Mechanosensitivity of the heart*. Dordrecht: Springer Netherlands; 2010. pp. 185–238. [https://doi.org/10.1007/978-90-481-2850-1\\_8](https://doi.org/10.1007/978-90-481-2850-1_8).
36. Andriulė I, Pangonytė D, Gwanyanya A, Karčiauskas D, Mubagwa K, Mačianskienė R. Detection of TRPM6 and TRPM7 proteins in normal and diseased Cardiac Atrial tissue and isolated cardiomyocytes. *Int J Mol Sci*. 2022;23:14860. <https://doi.org/10.3390/ijms232314860>.
37. Numata T, Shimizu T, Okada Y. TRPM7 is a stretch- and swelling-activated cation channel involved in volume regulation in human epithelial cells. *Am J Physiol Cell Physiol*. 2007;292:C460–467. <https://doi.org/10.1152/ajpcell.00367.2006>.
38. Bessac BF, Fleig A. TRPM7 channel is sensitive to osmotic gradients in human kidney cells. *J Physiol*. 2007;582:1073–86. <https://doi.org/10.1113/jphysiol.2007.130534>.
39. Oancea E, Wolfe JT, Clapham DE. Functional TRPM7 channels accumulate at the plasma membrane in response to fluid flow. *Circ Res*. 2006;98:245–53. <https://doi.org/10.1161/01.RES.0000200179.29375.cc>.
40. Riccio A, Medhurst AD, Mattei C, Kelsell RE, Calver AR, Randall AD, et al. mRNA distribution analysis of human TRPC family in CNS and peripheral tissues. *Brain Res Mol Brain Res*. 2002;109:95–104. [https://doi.org/10.1016/S0169-328X\(02\)00527-2](https://doi.org/10.1016/S0169-328X(02)00527-2).
41. Huang H, Liang L, Liu P, Wei H, Sachs F, Niu W, et al. Mechanical effects on KATP Channel Gating in Rat Ventricular myocytes. *PLoS ONE*. 2013;8:e63337. <https://doi.org/10.1371/journal.pone.0063337>.
42. Maroto R, Raso A, Wood TG, Kurosky A, Martinac B, Hamill OP. TRPC1 forms the stretch-activated cation channel in vertebrate cells. *Nat Cell Biol*. 2005;7:179–85. <https://doi.org/10.1038/ncb1218>.
43. Barritt G, Rychkov G. TRPs as mechanosensitive channels. *Nat Cell Biol*. 2005;7:105–7. <https://doi.org/10.1038/ncb0205-105>.
44. Liu H, El Zein L, Kruse M, Guinamad R, Beckmann A, Bozio A, et al. Gain-of-function mutations in TRPM4 cause autosomal dominant isolated cardiac conduction Disease. *Circ Cardiovasc Genet*. 2010;3:374–85. <https://doi.org/10.1161/CIRCGENETICS.109.930867>.
45. Guinamad R, Demion M, Magaud C, Potreau D, Bois P. Functional expression of the TRPM4 cationic current in ventricular cardiomyocytes from spontaneously hypertensive rats. *Hypertension*. 2006;48:587–94. <https://doi.org/10.1161/01.HYP.0000237864.65019.a5>.
46. Morita H, Honda A, Inoue R, Ito Y, Abe K, Nelson MT, et al. Membrane stretch-induced activation of a TRPM4-like nonselective cation channel in cerebral artery myocytes. *J Pharmacol Sci*. 2007;103:417–26. <https://doi.org/10.1254/jphs.fp0061332>.
47. Brayden JE, Earley S, Nelson MT, Reading S. Transient receptor potential (TRP) channels, vascular tone and autoregulation of cerebral blood flow. *Clin Exp Pharmacol Physiol*. 2008;35:1116–20. <https://doi.org/10.1111/j.1440-1681.2007.04855.x>.
48. Koch SE, Gao X, Haar L, Jiang M, Lasko VM, Robbins N, et al. Probenecid: novel use as a non-injurious positive inotrope acting via cardiac TRPV2 stimulation. *J Mol Cell Cardiol*. 2012;53:134–44. <https://doi.org/10.1016/j.yjmcc.2012.04.011>.
49. Muraki K, Iwata Y, Katanosaka Y, Ito T, Ohya S, Shigekawa M, et al. TRPV2 is a component of osmotically sensitive cation channels in murine aortic myocytes. *Circ Res*. 2003;93:829–38. <https://doi.org/10.1161/01.RES.0000097263.10220.0C>.
50. Fauconnier J, Lanner JT, Sultan A, Zhang S-J, Katz A, Bruton JD, et al. Insulin potentiates TRPC3-mediated cation currents in normal but not in insulin-resistant mouse cardiomyocytes. *Cardiovasc Res*. 2007;73:376–85. <https://doi.org/10.1016/j.cardiores.2006.10.018>.
51. Goel M, Zuo C-D, Sinkins WG, Schilling WP. TRPC3 channels colocalize with  $Na^+/Ca^{2+}$  exchanger and  $Na^+$  pump in axial component of transverse-axial tubular system of rat ventricle. *Am J Physiol Heart Circ Physiol*. 2007;292:874–83. <https://doi.org/10.1152/ajpheart.00785.2006>.
52. Kojima A, Kitagawa H, Omatsu-Kanbe M, Matsuura H, Nosaka S.  $Ca^{2+}$  paradox injury mediated through TRPC channels in mouse ventricular myocytes. *Br J Pharmacol*. 2010;161:1734–50. <https://doi.org/10.1111/j.1476-5381.2010.00986.x>.
53. Yamaguchi Y, Iribe G, Nishida M, Naruse K. Role of TRPC3 and TRPC6 channels in the myocardial response to stretch: linking physiology and

- pathophysiology. *Prog Biophys Mol Biol.* 2017;130:264–72. <https://doi.org/10.1016/j.pbiomolbio.2017.06.010>.
54. Han L, Li J. Canonical transient receptor potential 3 channels in atrial fibrillation. *Eur J Pharmacol.* 2018;837:1–7. <https://doi.org/10.1016/j.ejphar.2018.08.030>.
55. Quick K, Zhao J, Eijkelkamp N, Linley JE, Rugiero F, Cox JJ, et al. TRPC3 and TRPC6 are essential for normal mechanotransduction in subsets of sensory neurons and cochlear hair cells. *Open Biol.* 2012;2:120068. <https://doi.org/10.1098/rsob.120068>.
56. Zhao Y, Huang H, Jiang Y, Wei H, Liu P, Wang W, et al. Unusual localization and translocation of TRPV4 protein in cultured ventricular myocytes of the neonatal rat. *Eur J Histochem.* 2012;56:e32. <https://doi.org/10.4081/ejh.2012.e32>.
57. Loukin S, Zhou X, Su Z, Saimi Y, Kung C. Wild-type and brachyolmia-causing mutant TRPV4 channels respond directly to stretch force. *J Biol Chem.* 2010;285:27176–81. <https://doi.org/10.1074/jbc.M110.143370>.
58. Suzuki M, Mizuno A, Kodaira K, Imai M. Impaired pressure sensation in mice lacking TRPV4. *J Biol Chem.* 2003;278:22664–8. <https://doi.org/10.1074/jbc.M302561200>.
59. Suzuki M, Sato J, Kutsuwada K, Ooki G, Imai M. Cloning of a stretch-inhibitable nonselective cation channel. *J Biol Chem.* 1999;274:6330–5. <https://doi.org/10.1074/jbc.274.10.6330>.
60. Birder LA, Nakamura Y, Kiss S, Nealen ML, Barrick S, Kanai AJ, et al. Altered urinary bladder function in mice lacking the vanilloid receptor TRPV1. *Nat Neurosci.* 2002;5:856–60. <https://doi.org/10.1038/nn902>.
61. Grimm C, Kraft R, Sauerbruch S, Schultz G, Harteneck C. Molecular and functional characterization of the melastatin-related cation channel TRPM3. *J Biol Chem.* 2003;278:21493–501. <https://doi.org/10.1074/jbc.M300945200>.
62. Gomis A, Soriano S, Belmonte C, Viana F. Hypoosmotic- and pressure-induced membrane stretch activate TRPC5 channels. *J Physiol.* 2008;586:5633–49. <https://doi.org/10.1113/jphysiol.2008.161257>.
63. Sénatore S, Rami Reddy V, Séméria M, Perrin L, Lalevé N. Response to mechanical stress is mediated by the TRPA channel painless in the *Drosophila* heart. *PLoS Genet.* 2010;6:e1001088. <https://doi.org/10.1371/journal.pgen.1001088>.
64. Corey DP, García-Añoveros J, Holt JR, Kwan KY, Lin S-Y, Vollrath MA, et al. TRPA1 is a candidate for the mechanosensitive transduction channel of vertebrate hair cells. *Nature.* 2004;432:723–30. <https://doi.org/10.1038/nature03066>.
65. Kindt KS, Viswanath V, Macpherson L, Quast K, Hu H, Patapoutian A, et al. *Caenorhabditis elegans* TRPA-1 functions in mechanosensation. *Nat Neurosci.* 2007;10:568–77. <https://doi.org/10.1038/nn1886>.
66. Spassova MA, Hewavitharana T, Xu W, Soboloff J, Gill DL. A common mechanism underlies stretch activation and receptor activation of TRPC6 channels. *Proc Natl Acad Sci U S A.* 2006;103:16586–91. <https://doi.org/10.1073/pnas.0606894103>.
67. Takahashi K, Kakimoto Y, Toda K, Naruse K. Mechanobiology in cardiac physiology and Diseases. *J Cell Mol Med.* 2013;17:225–32. <https://doi.org/10.1111/jcmm.12027>.
68. Sharif-Naeini R, Folgering JHA, Bichet D, Duprat F, Lauritzen I, Arhatte M, et al. Polycystin-1 and -2 dosage regulates pressure sensing. *Cell.* 2009;139:587–96. <https://doi.org/10.1016/j.cell.2009.08.045>.
69. Foster DB, Gu J-M, Kim EH, Wolfson DW, O'Meally R, Cole RN, et al. Tbx18 orchestrates Cytoskeletal Transdifferentiation of Cardiomyocytes to Pacemaker cells by recruiting the epithelial-mesenchymal transition program. *J Proteome Res.* 2022;21:2277–92. <https://doi.org/10.1021/acs.jproteome.2c00133>.
70. Watanabe H, Murakami M, Ohba T, Ono K, Ito H. The pathological role of transient receptor potential channels in Heart Disease. *Circ J.* 2009;73:419–27. <https://doi.org/10.1253/circj.cj-08-1153>.
71. Gottlieb PA, Bae C, Sachs F. Gating the mechanical channel Piezo1: a comparison between whole-cell and patch recording. *Channels (Austin).* 2012;6:282–9. <https://doi.org/10.4161/chan.21064>.
72. Wong T-Y, Juang WC, Tsai CT, Tseng CJ, Lee WH, Chang SN, et al. Mechanical stretching simulates Cardiac Physiology and Pathology through Mechanosensor Piezo1. *J Clin Med.* 2018;7:410. <https://doi.org/10.3390/jcm7110410>.
73. Copp SW, Kim JS, Ruiz-Velasco V, Kaufman MP. The mechano-gated channel inhibitor GsMTx4 reduces the exercise pressor reflex in decerebrate rats. *J Physiol.* 2016;594:641–55. <https://doi.org/10.1113/JP271714>.
74. Zeng W-Z, Marshall KL, Min S, Daou I, Chapeau MW, Abboud FM, et al. PIEZO2 mediate neuronal sensing of blood pressure and the Baroreceptor Reflex. *Science.* 2018;362:464–7. <https://doi.org/10.1126/science.aau6324>.
75. Tan JHC, Liu W, Saint DA. Differential expression of the mechanosensitive potassium channel TREK-1 in epicardial and endocardial myocytes in rat ventricle. *Exp Physiol.* 2004;89:237–42. <https://doi.org/10.1113/expphysiol.2003.027052>.
76. Schmidt C, Wiedmann F, Kallenberger SM, Ratte A, Schulte JS, Scholz B, et al. Stretch-activated two-pore-domain (K2P) potassium channels in the heart: focus on atrial fibrillation and Heart Failure. *Prog Biophys Mol Biol.* 2017;130:233–43. <https://doi.org/10.1016/j.pbiomolbio.2017.05.004>.
77. Maingret F, Patel AJ, Lesage F, Lazdunski M, Honoré E. Mechano- or acid stimulation, two interactive modes of activation of the TREK-1 potassium channel. *J Biol Chem.* 1999;274:26691–6. <https://doi.org/10.1074/jbc.274.38.26691>.
78. Takahashi K, Naruse K. Stretch-activated BK channel and heart function. *Prog Biophys Mol Biol.* 2012;110:239–44. <https://doi.org/10.1016/j.pbiomolbio.2012.08.001>.
79. Sokabe M, Naruse K, Qiong-Yao T. A new mechanosensitive channel SAKCA and a new MS channel blocker GsTMx-4. *Nihon Yakurigaku Zasshi.* 2004;124:301–10. <https://doi.org/10.1254/fpj.124.301>.
80. Van Wagoner DR. Mechanosensitive gating of atrial ATP-sensitive potassium channels. *Circ Res.* 1993;72:973–83. <https://doi.org/10.1161/01.RES.0000147311.54833.03>.
81. Beyder A, Rae JL, Bernard C, Stregé PR, Sachs F, Farrugia G. Mechanosensitivity of Nav1.5, a voltage-sensitive sodium channel. *J Physiol.* 2010;588:4969–85. <https://doi.org/10.1113/jphysiol.2010.199034>.
82. Morris CE, Juranka PF. Nav Channel Mechanosensitivity: activation and inactivation accelerate reversibly with Stretch. *Biophys J.* 2007;93:822–33. <https://doi.org/10.1529/biophysj.106.101246>.
83. Wang JA, Lin W, Morris T, Banderali U, Juranka PF, Morris CE. Membrane trauma and Na<sup>+</sup> leak from Nav1.6 channels. *Am J Physiol Cell Physiol.* 2009;297:C823–834. <https://doi.org/10.1152/ajpcell.00505.2008>.
84. Lyford GL, Stregé PR, Shepard A, Ou Y, Ermilov L, Miller SM, et al. Alpha (1.2) (ca(V)1.2) L-type calcium channel mediates mechanosensitive calcium regulation. *Am J Physiol Cell Physiol.* 2002;283:C1001–1008. <https://doi.org/10.1152/ajpcell.00140.2002>.
85. Vincent PF, Bouleau Y, Petit C, Dulon D. A synaptic F-actin network controls otoferlin-dependent exocytosis in auditory inner hair cells. *Elife.* 2015;4:e10988. <https://doi.org/10.7554/eLife.10988>.
86. Calabrese B, Tabarean IV, Juranka P, Morris CE. Mechanosensitivity of N-type calcium channel currents. *Biophys J.* 2002;83:2560–74. [https://doi.org/10.1016/S0006-3495\(02\)75267-3](https://doi.org/10.1016/S0006-3495(02)75267-3).
87. Laitko U, Morris CE. Membrane tension accelerates rate-limiting voltage-dependent activation and slow inactivation steps in a Shaker channel. *J Gen Physiol.* 2004;123:135–54. <https://doi.org/10.1085/jgp.200308965>.
88. Hammami S, Willumsen NJ, Olsen HL, Morera FJ, Latorre R, Klaerke DA. Cell volume and membrane stretch independently control K<sup>+</sup> channel activity. *J Physiol.* 2009;587:2225–31. <https://doi.org/10.1113/jphysiol.2008.163550>.
89. Grunnet M, Jørgensen T, MacAulay N, Jørgensen NK, Schmitt N, Pongs O, et al. KCNQ1 channels sense small changes in cell volume. *J Physiol.* 2003;549:419–27. <https://doi.org/10.1113/jphysiol.2003.038455>.
90. Otway R, Vandenberg JJ, Guo G, Varghese A, Castro ML, Liu J, et al. Stretch-sensitive KCNQ1 mutation A link between genetic and environmental factors in the pathogenesis of atrial fibrillation? *J Am Coll Cardiol.* 2007;49:578–86. <https://doi.org/10.1016/j.jacc.2006.09.044>.
91. Fatehi M, Carter CC, Youssef N, Light PE. The mechano-sensitivity of cardiac ATP-sensitive potassium channels is mediated by intrinsic MgATPase activity. *J Mol Cell Cardiol.* 2017;108:34–41. <https://doi.org/10.1016/j.yjmcc.2017.05.004>.
92. Al-Shammari H, Latif N, Sarathchandra P, McCormack A, Rog-Zielinska EA, Raja S, et al. Expression and function of mechanosensitive ion channels in human valve interstitial cells. *PLoS ONE.* 2020;15:e0240532. <https://doi.org/10.1371/journal.pone.0240532>.
93. Maingret F, Patel AJ, Lesage F, Lazdunski M, Honoré E. Lysophospholipids open the two-pore domain mechano-gated K(+) channels TREK-1 and TRAAK. *J Biol Chem.* 2000;275:10128–33. <https://doi.org/10.1074/jbc.275.14.10128>.
94. Numata T, Shimizu T, Okada Y. Direct mechano-stress sensitivity of TRPM7 channel. *Cell Physiol Biochem.* 2007;19:1–8. <https://doi.org/10.1159/000099187>.
95. Earley S, Waldron BJ, Brayden JE. Critical role for transient receptor potential channel TRPM4 in myogenic constriction of cerebral arteries. *Circ Res.* 2004;95:922–9. <https://doi.org/10.1161/01.RES.0000147311.54833.03>.
96. Yamaguchi Y, Iribe G, Kaneko T, Takahashi K, Numaga-Tomita T, Nishida M, et al. TRPC3 participates in angiotensin II type 1 receptor-dependent stress-induced slow increase in intracellular Ca<sup>2+</sup> concentration in mouse



- cardiomyocytes. *J Physiol Sci.* 2018;68:153–64. <https://doi.org/10.1007/s12576-016-0519-3>.
97. Christensen AP, Corey DP. TRP channels in mechanosensation: direct or indirect activation? *Nat Rev Neurosci.* 2007;8:510–21. <https://doi.org/10.1038/nrn2149>.
98. Bae C, Sachs F, Gottlieb PA. The mechanosensitive ion channel Piezo1 is inhibited by the peptide GsMTx4. *Biochemistry.* 2011;50:6295–300. <https://doi.org/10.1021/bi200770q>.
99. Bae C, Gottlieb PA, Sachs F. Human PIEZO1: removing inactivation. *Biophys J.* 2013;105:880–6. <https://doi.org/10.1016/j.bpj.2013.07.019>.
100. Josephson I, Sperelakis N. On the ionic mechanism underlying adrenergic-cholinergic antagonism in ventricular muscle. *J Gen Physiol.* 1982;79:69–86. <https://doi.org/10.1085/jgp.79.1.69>.
101. Kamkin A, Kiseleva I, Theres H, Eulert-Grehn J-J, Wagner KD, Scholz H, et al. Enhanced L-type calcium currents in cardiomyocytes from transgenic rats overexpressing SERCA2a. *Exp Clin Cardiol.* 2010;15:e109–15.
102. Monteilh-Zoller MK, Hermosura MC, Nadler MJS, Scharenberg AM, Penner R, Fleig A. TRPM7 provides an ion channel mechanism for cellular entry of trace metal ions. *J Gen Physiol.* 2003;121:49–60. <https://doi.org/10.1085/jgp.20028740>.
103. Nadler MJ, Hermosura MC, Inabe K, Perraud AL, Zhu Q, Stokes AJ, et al. LTRPC7 is a Mg-ATP-regulated divalent cation channel required for cell viability. *Nature.* 2001;411:590–5. <https://doi.org/10.1038/35079092>.
104. Zitt C, Zobel A, Obukhov AG, Harteneck C, Kalkbrenner F, Lückhoff A, et al. Cloning and functional expression of a human Ca<sup>2+</sup>-permeable cation channel activated by calcium store depletion. *Neuron.* 1996;16:1189–96. [https://doi.org/10.1016/s0896-6273\(00\)80145-2](https://doi.org/10.1016/s0896-6273(00)80145-2).
105. Dienes C, Hézső T, Kiss DZ, Baranyai D, Kovács ZM, Szabó L, et al. Electrophysiological effects of the Transient Receptor Potential Melastatin 4 Channel Inhibitor (4-Chloro-2-(2-chlorophenoxy)acetamido) Benzoic Acid (CBA) in Canine Left Ventricular Cardiomyocytes. *Int J Mol Sci.* 2021;22:9499. <https://doi.org/10.3390/ijms22179499>.
106. Hof T, Simard C, Rouet R, Sallé L, Guinamard R. Implication of the TRPM4 nonselective cation channel in mammalian sinus rhythm. *Heart Rhythm.* 2013;10:1683–9. <https://doi.org/10.1016/j.hrthm.2013.08.014>.
108. Zaritsky JJ, Redell JB, Tempel BL, Schwarz TL. The consequences of disrupting cardiac inwardly rectifying K<sup>+</sup> current (*I<sub>K1</sub>*) as revealed by the targeted deletion of the murine Kir2.1 and Kir2.2 genes. *J Physiol.* 2001;533:697–710. <https://doi.org/10.1111/j.1469-7793.2001.t01-1-00697.x>.
109. Clark RB, Tremblay A, Melnyk P, Allen BG, Giles WR, Fiset C. T-tubule localization of the inward-rectifier K<sup>+</sup> channel in mouse ventricular myocytes: a role in K<sup>+</sup> accumulation. *J Physiol.* 2001;537:979–92. <https://doi.org/10.1111/j.1469-7793.2001.00979.x>.
109. Scherer D, Seyler C, Xynogalos P, Scholz EP, Thomas D, Backs J, et al. Inhibition of Cardiac Kir Current (*I<sub>K1</sub>*) by protein kinase C critically depends on PKCβ and Kir2.2. *PLoS ONE.* 2016;11:e0156181. <https://doi.org/10.1371/journal.pone.0156181>.
110. Isenberg G, Kondratev D, Dyachenko V, Kazanski V, Gallitelli MF. Isolated cardiomyocytes: Mechanosensitivity of Action potential, membrane current and Ion Concentration. In: Kamkin A, Kiseleva I, editors. *Mechanosensitivity in cells and tissues.* Moscow: Academia; 2005. <http://www.ncbi.nlm.nih.gov/books/NBK7515/>.
111. Tabarean IV, Juranka P, Morris CE. Membrane stretch affects gating modes of a skeletal muscle sodium channel. *Biophys J.* 1999;77:758–74. [https://doi.org/10.1016/S0006-3495\(99\)76930-4](https://doi.org/10.1016/S0006-3495(99)76930-4).
112. Laitko U, Juranka PF, Morris CE. Membrane stretch slows the concerted step prior to opening in a kv channel. *J Gen Physiol.* 2006;127:687–701. <https://doi.org/10.1085/jgp.200509394>.
113. Lab MJ. Mechanosensitive-mediated interaction, integration, and cardiac control. *Ann N Y Acad Sci.* 2006;1080:282–300. <https://doi.org/10.1196/annals.1380.022>.
114. Janmey PA. The cytoskeleton and cell signaling: component localization and mechanical coupling. *Physiol Rev.* 1998;78:763–81. <https://doi.org/10.1152/physrev.1998.78.3.763>.
115. Dabiri BE, Lee H, Parker KK. A potential role for integrin signaling in mechano-electrical feedback. *Prog Biophys Mol Biol.* 2012;10:196–203. <https://doi.org/10.1016/j.pbiomolbio.2012.07.002>.
116. Kamkin AG, Kamkina OV, Shim AL, Bilichenko A, Mitrokhin VM, Kazansky VE, et al. The role of activation of two different sGC binding sites by NO-dependent and NO-independent mechanisms in the regulation of SACs in rat ventricular cardiomyocytes. *Physiol Rep.* 2022;10:e15246. <https://doi.org/10.14814/phy2.15246>.
117. Petroff MG, Kim SH, Pepe S, Dessy C, Carbán E, Balligand JL, et al. Endogenous nitric oxide mechanisms mediate the stretch dependence of Ca<sup>2+</sup> release in cardiomyocytes. *Nat Cell Biol.* 2001;3:867–73. <https://doi.org/10.1038/ncb1001-867>.
118. Ehara T, Noma A, Ono K. Calcium-activated non-selective cation channel in ventricular cells isolated from adult guinea-pig hearts. *J Physiol.* 1988;403:117–33.
119. Gannier F, White E, Le Garnier null JY. A possible mechanism for large stretch-induced increase in [Ca<sup>2+</sup>]<sub>i</sub> in isolated guinea-pig ventricular myocytes. *Cardiovasc Res.* 1996;32:158–67.
120. Isenberg G, Kazanski V, Kondratev D, Gallitelli MF, Kiseleva I, Kamkin A. Differential effects of stretch and compression on membrane currents and [Na<sup>+</sup>]<sub>c</sub> in ventricular myocytes. *Prog Biophys Mol Biol.* 2003;82:43–56. [https://doi.org/10.1016/s0079-6107\(03\)00004-x](https://doi.org/10.1016/s0079-6107(03)00004-x).
121. Wendt-Gallitelli MF, Voigt T, Isenberg G. Microheterogeneity of subsarcolemmal sodium gradients. Electron probe microanalysis in guinea-pig ventricular myocytes. *J Physiol.* 1993;472:33–44. <https://doi.org/10.1113/jphysiol.1993.sp019934>.
122. Yang XC, Sachs F. Block of stretch-activated ion channels in *Xenopus* oocytes by gadolinium and calcium ions. *Science.* 1989;243:1068–71. <https://doi.org/10.1126/science.2466333>.
123. Tang QY, Qi Z, Naruse K, Sokabe M. Characterization of a functionally expressed stretch-activated BK<sub>ca</sub> channel cloned from chick ventricular myocytes. *J Membr Biol.* 2003;196:185–200. <https://doi.org/10.1007/s00232-003-0637-8>.
124. Hongo K, Pascarel C, Cazorla O, Gannier F, Le Guennec JY, White E. Gadolinium blocks the delayed rectifier potassium current in isolated guinea-pig ventricular myocytes. *Exp Physiol.* 1997;82:647–56. <https://doi.org/10.1113/expphysiol.1997.sp004053>.
125. Lacampagne A, Gannier F, Argibay J, Garnier D, Le Guennec JY. The stretch-activated ion channel blocker gadolinium also blocks L-type calcium channels in isolated ventricular myocytes of the guinea-pig. *Biochim Biophys Acta.* 1994;1191:205–8. [https://doi.org/10.1016/0005-2736\(94\)90250-x](https://doi.org/10.1016/0005-2736(94)90250-x).

## Publisher's Note

Springer Nature remains neutral with regard to jurisdictional claims in published maps and institutional affiliations.